

The Kirkwood-Bethe hypothesis for bubble dynamics, cavitation and underwater explosions

Fabian Denner^{1, a)}

Department of Mechanical Engineering, Polytechnique Montréal, Montréal, H3T 1J4, Québec, Canada

Pressure-driven bubble dynamics is a major topic of current research in fluid dynamics, driven by innovative medical therapies, sonochemistry, material treatments, and geophysical exploration. First proposed in 1942, the Kirkwood-Bethe hypothesis provides a simple means to close the equations that govern pressure-driven bubble dynamics as well as the resulting flow field and acoustic emissions in spherical symmetry. The models derived from the Kirkwood-Bethe hypothesis can be solved using standard numerical integration methods at a fraction of the computational cost required for fully resolved simulations. Here, the theoretical foundation of the Kirkwood-Bethe hypothesis and contemporary models derived from it are gathered and reviewed, as well as generalized to account for spherically symmetric, cylindrically symmetric, and planar one-dimensional domains. In addition, the underpinning assumptions are clarified and new results that scrutinize the predictive capabilities of the Kirkwood-Bethe hypothesis with respect to the complex acoustic impedance experienced by curved acoustic waves and the formation of shock waves are presented. Although the Kirkwood-Bethe hypothesis is built upon simplifying assumptions and lacks some basic acoustic properties, models derived from it are able to provide accurate predictions under the specific conditions associated with pressure-driven bubble dynamics, cavitation and underwater explosions.

Copyright (2024) Author(s). This article is distributed under a Creative Commons Attribution (CC BY) License.

I. INTRODUCTION

Pressure-driven bubble dynamics are encountered and play an important role in countless engineering applications and natural phenomena¹⁻³. The formation and collapse of vapor bubbles (*cf.* hydrodynamic cavitation) are well known to cause material erosion of propellers and hydro turbines⁴⁻⁶, and the related acoustic emissions are actively studied and monitored *in situ*⁷⁻⁹. However, the past decades have seen a paradigm shift in how pressure-driven bubble dynamics and, especially, cavitation are studied, away from treating cavitation solely as a hazard, towards leveraging its mechanical and thermal effects. This has spawned innovative new applications, such as contrast-enhanced medical imaging¹⁰, intensifying chemical reactions¹¹, breaking down kidney and urinary stones^{12,13}, treating tumors¹⁴, using cavitation as a sonic scalpel for precision surgery^{15,16}, targeted drug delivery by ultrasound-driven micro- and nanobubbles¹⁷, 3D printing with sound¹⁸, actuating smart materials¹⁹, and enhancing bioadhesion²⁰. The energy focused by a strong bubble collapse can be utilized to pierce biological cells^{21,22}, to destruct bacteria for wastewater treatment²³, to clean surfaces and membranes^{24,25}, to synthesize nanoparticles and nanostructured materials²⁶, and to manipulate hardened materials, such as metals²⁷ and glass²⁸. Ferns use cavitation-driven catapults to eject their spores²⁹ and pistol shrimps use the shock waves generated by collapsing bubbles to stun their prey³⁰. The pressure and shock waves of underwater explosions are studied for defense purposes as a major

component of marine warfare³¹⁻³³ and the pressure transients produced by the generation and collapse of underwater bubbles are used for seismic surveys in marine and geophysical exploration³⁴⁻³⁶. The advent of modern monitoring and control techniques for bubble dynamics, many of which now leverage machine learning algorithms, largely rely on acoustic signals to identify and classify bubble activity^{8,37-42}. This, in turn, requires high-fidelity models of the complex bubble dynamics and nonlinear acoustics to classify the related acoustic signatures and to train machine learning algorithms.

The *Kirkwood-Bethe hypothesis*⁴³ is an important tool for fundamental and theoretical research on pressure-driven bubble dynamics, as well as the related fluid dynamics and acoustics. It stipulates that in spherical symmetry the quantity

$$g = r \left(h - h_\infty + \frac{u^2}{2} \right), \quad (1)$$

emitted at the gas-liquid interface of a gas cavity or bubble, is constant along outgoing characteristics and propagates with speed $c + u$, where r is the radial coordinate, c is the liquid speed of sound, u is the flow velocity, and $h - h_\infty$ is the difference in specific enthalpy between radial location r and the ambient state denoted with subscript ∞ . The power of the Kirkwood-Bethe hypothesis lies in the fact that it enables, in conjunction with a suitable equation of state, to close the set of equations governing the pressure-driven behavior of gas bubbles and the resulting flow of the surrounding liquid, such that mathematical models for the velocity and pressure generated by a cavitation bubble or an underwater explosion can be derived. Computer programs developed in the 1960s using models for pressure-driven bubble dynamics and acoustics based on the Kirkwood-Bethe hypoth-

^{a)} fabian.denner@polymtl.ca

esis were also among the first open-source software tools in fluid dynamics^{44,45}. Despite the widespread availability of simulation tools that can predict two- and three-dimensional pressure-driven bubble dynamics in complex scenarios with increasing accuracy and robustness^{46–50}, the Kirkwood-Bethe hypothesis and the models derived from it, henceforth collectively referred to as *KBH models*, still play an important role for the prediction of pressure-driven bubble phenomena. Predicting the dynamic behavior of collapsing bubbles and the pressure transients they produce remains challenging and KBH models have emerged as robust benchmarks for testing and validating these numerical methods^{50–54}. In addition, acoustic emissions can be modulated by different mechanisms^{55–57} and, consequently, interpreting acoustic signals at a distance remains a complex task. To this end, the Kirkwood-Bethe hypothesis has seen a renewed interest over the past years as the basis for gaining an improved understanding of the interaction between acoustic emissions and fluid dynamics^{57–61}, primarily in relation to pressure-driven bubble dynamics.

Although the Kirkwood-Bethe hypothesis and models are well established and widely used today, much of their theoretical foundation is scattered over many institutional reports^{45,62–66}, declassified military reports^{67–71}, textbooks^{31,72–74}, PhD theses^{44,75}, and papers^{76–82} published in the years and decades following the report of Kirkwood and Bethe⁴³. Many of these formidable works are difficult to obtain and are, thus, often not credited correctly or even overlooked in the modern literature. Further adding to the difficulties associated with gaining a comprehensive picture of the Kirkwood-Bethe hypothesis and models, the original report of Kirkwood and Bethe⁴³ does not appear to be indexed in scientific databases, meaning that a list of subsequent publications referencing this report is not readily available, and no review of the scientific literature related to the Kirkwood-Bethe hypothesis has been published.

The aim of this review is to gather, for the first time, the theoretical foundation of the Kirkwood-Bethe hypothesis, as well as models derived from it that are still relevant today, in a single document. Moreover, the description of the flow field arising from the Kirkwood-Bethe hypothesis is further generalized and the analysis of the limitations and assumptions underpinning the Kirkwood-Bethe hypothesis is extended.

As a first step, Section II provides a short historical overview of major developments and applications related to the Kirkwood-Bethe hypothesis. Subsequently, the Kirkwood-Bethe hypothesis is derived from the conservation laws governing mass, momentum and energy in Section III, paying particular attention to the underpinning assumptions. The application of different equations of state describing the properties of the liquid is presented in Section IV, the equation of motion of the gas-liquid interface of a pressure-driven gas bubble or cavity is presented in Section V, and models to describe the flow generated by oscillating or collapsing bubbles and cavities are de-

rived in Section VI. The model hierarchy with respect to the Mach number following from the Kirkwood-Bethe hypothesis is briefly reviewed in Section VII and numerical methods to solve KBH models for the bubble dynamics, flow field and shock waves are discussed in Section VIII. In Section IX, the assumptions and capabilities of the Kirkwood-Bethe hypothesis are further scrutinized and new results are presented. Conclusions are drawn and open questions are discussed in Section X.

II. RETROSPECTIVE

The Kirkwood-Bethe hypothesis was proposed as part of a technical report⁴³ commissioned by the research office of the United States federal government on predicting the pressure wave produced by an underwater explosion, completed in 1942 by John G. Kirkwood and Hans A. Bethe. This report focused on obtaining an approximation for the pressure amplitude at some distance from an underwater explosion and, more precisely, the decay constant describing an approximately exponential decay of the peak pressure. To this end, Kirkwood and Bethe focused on the propagation of the shock front, the conditions in the liquid behind the shock front, the rapidly expanding gas bubble of burnt detonation products, and the rarefaction wave forming inside the gas bubble. The work of Kirkwood and Bethe was first brought to the attention of a wider audience through the textbook of Cole³¹.

A. Theoretical foundations

Shortly after its publication, Rice and Ginell^{67,68} extended the work of Kirkwood and Bethe⁴³ to an explosive charge in the shape of an infinite cylinder by considering cylindrical instead of spherical symmetry. Although they found that the Kirkwood-Bethe hypothesis is less accurate in cylindrical symmetry than it is in spherical symmetry, it provided a first glimpse into the dynamics of underwater explosions that are not spherically symmetric. The work of Rice and Ginell^{67,68} later became the foundation of the studies of Naugol'nykh and Roy⁷¹ on the hydrodynamics of electrical discharges in liquids and of Kedrinskii⁸⁰ on cylindrically symmetric underwater explosions.

In 1952, Gilmore⁶² studied the Kirkwood-Bethe hypothesis further, focusing, however, on cavitation bubble dynamics rather than on underwater explosions. Aside from clarifying some assumptions and exploring the theoretical limits of the Kirkwood-Bethe assumption, Gilmore presented a second-order differential equation of the radial motion of the gas-liquid interface of a spherical gas bubble in a compressible fluid as a result of ambient pressure differences, now known as the *Gilmore model*, which has since become a staple of fundamental research on cavitation. As it contains important terms that are second order with respect to the Mach number of the

gas-liquid interface motion, the Gilmore model presents an extension to the models of Herring⁸³ and Trilling⁸⁴ that are bound to first-order acoustics. In addition, Gilmore⁶² also derived models for the flow velocity and pressure induced by a bubble or cavity under different assumptions. Among these models is an ordinary differential equation (ODE) for the flow velocity with respect to the radial coordinate along outgoing characteristics based on the Kirkwood-Bethe hypothesis, which allows to reconstruct the flow and acoustics resulting from a bubble collapse or oscillation. Generalizing the Gilmore model for spherical bubbles, Kedrinskii and Kuzavov⁸⁵ proposed a model of the radial dynamics of bubbles in planar and cylindrical symmetry.

Hickling and Plesset⁶⁴ published an institutional report on a study of the collapse and rebound of an adiabatically compressed gas cavity in 1963, using the Kirkwood-Bethe hypothesis in conjunction with the method of characteristics. A shortened version of their report was published as a paper⁷⁶ the following year. To describe the flow of the liquid surrounding the gas cavity, Hickling and Plesset presented ODEs for both the flow velocity and pressure with respect to time along outgoing characteristics based on the Kirkwood-Bethe hypothesis, although they did not present a detailed derivation of these ODEs. Under the assumptions associated with the Kirkwood-Bethe hypothesis, the ODE for the flow velocity with respect to time (du/dt) proposed by Hickling and Plesset⁶⁴ is equivalent to the ODE with respect to the radial coordinate (du/dr) of Gilmore⁶².

Ivany⁴⁴ revisited the theory on cavitation bubble dynamics and acoustic emissions in a PhD thesis on the collapse of gas cavities, completed in 1965. In this thesis, which was in parts published in a subsequent paper⁷⁷, Ivany presented a detailed derivation of an ODE for the flow velocity in the liquid starting from the momentum and continuity equations by using the Kirkwood-Bethe hypothesis and, in fact, arrived at the same ODE as Hickling and Plesset⁶⁴ two years prior. However, while the model presented by Hickling and Plesset required to also solve an ODE for the pressure, Ivany employed an explicit expression for the pressure along outgoing characteristics obtained directly from the Kirkwood-Bethe hypothesis using the Tait⁸⁶ equation of state (EoS), as previously suggested by Gilmore⁶². In the appendix of the thesis, Ivany⁴⁴ carefully explains how the bubble dynamics and the flow field are solved and, remarkably, provides listings of the developed computer codes, written in the *Michigan Algorithm Decoder* programming language, making it perhaps the first open-source software for cavitation research. Shortly after, in 1966, Lilliston⁴⁵ provided a computer code written in *Fortran IV* for bubble dynamics and the resulting flow field based on the work of Gilmore⁶² in the appendix of a report on the collapse of a gas-filled cavity.

Akulichev *et al.*⁷⁹ proposed an explicit approximation for the pressure emitted by oscillating bubbles using Riemann invariants and the Tait EoS on the basis of the

Kirkwood-Bethe hypothesis, which does not require explicit knowledge of the generated flow velocity. Moreover, while previous studies^{44,62,64} had deliberately avoided the multivalued solutions arising at shock fronts, Akulichev *et al.*⁷⁹ used the *rule of equal areas*⁸⁷ to treat such multivalued solutions. As a result, Akulichev and co-workers were able to demonstrate that when the emitted pressure wave forms a shock front, the pressure may be severely overpredicted if the additional dissipation arising at the shock front is not taken into account.

All the research reported in the publications discussed above employ the (modified) Tait equation of state⁸⁶ to describe the liquid properties, starting with the original work of Kirkwood and Bethe⁴³. The main shortcoming of the Tait EoS is that it drastically overpredicts the temperature due to isentropic compression^{88–90}. However, the Kirkwood-Bethe hypothesis is not limited to a specific EoS for the liquid. Flynn^{63,66} used a tabulated EoS based on the work of Rice and Walsh⁹¹ to define the properties of the liquid. Unfortunately, however, a copy of one of Flynn's reports⁶³ on this matter could not be located (the reference here relies on the account of Ivany⁴⁴), while the other report⁶⁶ does not present the methodology in detail. Recently, Denner⁹⁰ extended the Gilmore model using the Noble-Abel stiffened-gas (NASG) EoS and, subsequently, Denner and Schenke⁶⁰ used the NASG EoS successfully to model the flow and acoustics induced by cavitation bubbles in conjunction with the models of Gilmore⁶², Hickling and Plesset⁶⁴, and Ivany⁴⁴.

These milestones form the foundation of KBH models today. Concurrent and subsequent research efforts have primarily focused on applying these models to various engineering problems, as well as to elucidate the physics of pressure-driven bubble dynamics and acoustics.

B. Applications

The application in the context of which the Kirkwood-Bethe hypothesis was originally conceived are underwater explosions, whereby the expansion of burnt gaseous detonation products and the emitted shock wave in the water are of primary interest. Early work on this subject, starting with the study of Kirkwood and Bethe⁴³, focused on predicting the evolution and decay of the peak pressure of the emitted shock wave in spherical^{43,92–98} and cylindrical symmetry^{67,68,80,99}. To this end, the main aim was to find an accurate definition for the decay constant θ of the approximately exponential decay, $e^{-t/\theta}$, of the peak pressure. In the 21st century, the focus has shifted away from approximating the peak pressure in favor of using KBH models to compute and study the full range of dynamics arising in underwater explosions, including the associated bubble dynamics^{100–103}, pressure and shock waves^{100,104}, and fluid-structure interaction¹⁰⁵. These models have repeatedly been found to be of very high predictive quality^{101–104}. The research into underwater

explosions is closely related to subsequent applications of the Kirkwood-Bethe hypothesis and, especially, the Gilmore model to predict the bubble dynamics of seismic air guns for geophysical exploration and the shock testing of defense vessels^{34,106–108}. For instance, Landrø and Sollie¹⁰⁹ proposed a methodology based on the Kirkwood-Bethe hypothesis to determine the pressure transients produced by an array of air guns, the results of which Laws, Landrø, and Amundsen¹¹⁰ found to be in very good agreement with measurements in different experimental scenarios. Similar methods to predict the pressure field produced by air guns were proposed by Ziolkowski^{106,107}. KBH models were also leveraged to study the influence of rough seas¹¹¹ and shallow water¹¹² on the acoustic signatures of seismic air guns.

Other applications in which a strong local energy deposition produces a gaseous bubble that emits pressure waves, and subsequently collapses and rebounds, are cavitation bubbles induced by an electrical discharge or a focused laser beam. Especially laser-induced cavitation has established itself as a widely-used tool to study cavitation bubble dynamics^{53,113–122} under controllable, precise, and reproducible conditions, both experimentally and computationally. Mellen⁷⁸ was an early adopter of the Kirkwood-Bethe hypothesis in the 1950s, in the form of the Gilmore model, to provide a theoretical basis for an experimental study of the evolution of a spherical cavity produced by an electrical discharge, reporting an encouraging agreement between experimental measurements and computational results. With respect to laser-induced cavitation, KBH models have been used, aside from studying the resulting bubble dynamics, to understand and quantify the formation and attenuation of shock waves^{58,59,61,123–128} and the energy partitioning^{59,61}. The results produced by these models have been shown to be in excellent agreement with experimental measurements^{58,61,125,126,129}.

A major driver of research into pressure-driven bubble dynamics over the past decades have been diagnostic and therapeutic medical applications. In 1984, Vacher, Gimenez, and Goutte¹³⁰ used the Gilmore model to show that ultrasound-driven bubbles emit significant energy at the second harmonic of the driving frequency, now a widely used indicator to detect and classify cavitation in medical ultrasound treatments¹³¹. Since then, KBH models have been used to study tissue ablation^{132–134}, histotripsy^{135–137} and lithotripsy¹³⁸ treatments, laser surgery^{124,128}, and ultrasound-driven encapsulated microbubbles, including their dynamic behavior^{133,139–143}, bubble-bubble interactions¹⁴⁴ and the associated acoustic emissions^{141,142}. To this end, Gümmer, Schenke, and Denner¹⁴² showed a favorable comparison of the frequency spectrum predicted by the Gilmore model for lipid-coated microbubbles with the experimental measurements of Song, Moldovan, and Prentice¹⁴⁵. To account for the viscoelastic rheology of tissue, Zilonova, Solovchuk, and Sheu^{146,147} extended the Gilmore model to include the linear elastic solid model, also known as

the Zener model, resulting in a markedly different bubble behavior^{143,146,147}.

The Kirkwood-Bethe hypothesis has also been utilized to study other applications of pressure-driven bubble dynamics, including food processing¹⁴⁸, the spall formation in aluminium¹⁴⁹, the treatment of materials^{150,151}, material synthesis^{26,152,153}, the preferred nucleation of crystals during solidification¹⁵⁴, surface cleaning¹⁵⁵, as well as the dynamics of a collapsing cylindrical cavity driven by an annular piston¹⁵⁶. Studies on sonoluminescence, whereby ultrasound-driven bubbles emit a light pulse upon collapse¹⁵⁷, have also directly benefited from KBH models, for instance to estimate the conditions insight the bubble during collapse^{158–160} and to correlate acoustic measurements to bubble dynamics^{161–163}. Aside from specific applications, KBH models have been used extensively to study and elucidate fundamental pressure-driven bubble dynamics and acoustics. Some examples of studies using the Gilmore model to study pressure-driven bubble dynamics include studies on the natural bubble frequency¹⁶⁴, self-similar bubble behavior^{165,166}, period doubling of ultrasound-driven bubbles¹⁶⁶, the excitation of bubbles with multiple frequencies¹⁶⁷, as well as the influence of the liquid compressibility¹⁶⁸, heat transfer¹⁶⁹, the vapor content¹⁷⁰, and a narrow confinement¹⁷¹ on the bubble dynamics. Moreover, the Kirkwood-Bethe hypothesis has been used to gain quantitative insight into the acoustic emissions associated with pressure-driven bubble dynamics, such as the acoustic noise spectrum generated by pressure-driven bubbles close to a free surface^{172,173}, the acoustic translation of bubbles¹⁷⁴, and the pressure and shock waves emitted during a strong bubble collapse^{58–61,163}.

III. THE KIRKWOOD-BETHE HYPOTHESIS

The Kirkwood-Bethe hypothesis can be derived using basic fluid dynamics, and the arising definitions and expressions then allow us to close the system of governing equations. In the following, we start in Section III A by bringing the conservation laws governing a fluid flow into a convenient form. Subsequently, the Kirkwood-Bethe hypothesis is derived in Section III B and its major limitations are discussed in Section III C.

A. Governing conservation laws

The conservation of mass, momentum and energy governing a fluid flow are given as

$$\frac{D\rho}{Dt} + \rho \nabla \cdot \mathbf{u} = 0 \quad (2)$$

$$\frac{D\mathbf{u}}{Dt} + \frac{1}{\rho} \nabla p = \frac{1}{\rho} \nabla \cdot \boldsymbol{\tau} \quad (3)$$

$$\frac{Dh}{Dt} - \frac{1}{\rho} \frac{Dp}{Dt} = \frac{1}{\rho} (\boldsymbol{\tau} : \nabla \mathbf{u} - \nabla \cdot \dot{q}), \quad (4)$$

where ρ is the fluid density, \mathbf{u} is the flow velocity, p denotes the pressure, h is the specific enthalpy, $\boldsymbol{\tau}$ represents viscous stresses, \dot{q} is the heat flux due to thermal conduction, and

$$\frac{D}{Dt} = \frac{\partial}{\partial t} + (\mathbf{u} \cdot \nabla) \quad (5)$$

denotes the material derivative operator. The thermodynamic relation $dh = T ds + dp/\rho$ allows us to reformulate the energy equation in terms of the specific entropy s , such that

$$\frac{Ds}{Dt} = \frac{1}{\rho T} (\boldsymbol{\tau} : \nabla \mathbf{u} - \nabla \cdot \dot{q}), \quad (6)$$

where T is the temperature. This system of equations is closed with a suitable equation of state (EoS) that defines a relationship between the thermodynamic quantities. Since the subsequent derivation is agnostic to the applied EoS, we proceed without assuming a specific EoS and revisit commonly used EoS in Section IV.

Assuming that the considered flow is ideal, without viscous dissipation ($\boldsymbol{\tau} = 0$) and heat conduction ($\dot{q} = 0$), we obtain the Euler equations:

$$\frac{D\rho}{Dt} + \rho \nabla \cdot \mathbf{u} = 0 \quad (7)$$

$$\frac{D\mathbf{u}}{Dt} + \frac{1}{\rho} \nabla p = 0 \quad (8)$$

$$\frac{Ds}{Dt} = 0. \quad (9)$$

This set of governing equations, with which Kirkwood and Bethe⁴³ commenced their work, assumes that changes to the state of the fluid of a sufficiently smooth flow are adiabatic and reversible. Consequently, the flow is *isentropic*, as imposed by Eq. (9). Especially for water, this turns out to be a good assumption even for pressure waves with a large amplitude, because the resulting change in entropy is small. The previously suggested upper limit for the validity of this approximation is $p = \mathcal{O}(\text{GPa})$.^{43,76} Assuming that the flow is isentropic does, however, not imply that all fluid elements are on the same isentrope, because the entropy may change at a shock front, which is further discussed in Section VIII C.

The differential relation of the specific enthalpy for an isentropic fluid is

$$dh = \frac{dp}{\rho} = c^2 \frac{d\rho}{\rho}, \quad (10)$$

with the speed of sound c defined as

$$c^2 = \left(\frac{\partial p}{\partial \rho} \right)_s, \quad (11)$$

where subscript s implies a constant entropy. In addition, to account for a time-varying pressure in the far field, we introduce the ambient enthalpy h_∞ and redefine, in a slight abuse of notation, the specific enthalpy difference

as $h \rightarrow h - h_\infty$. The ambient enthalpy h_∞ is spatially invariant ($\nabla h_\infty = 0$), such that

$$\frac{Dh_\infty}{Dt} = \frac{\partial h_\infty}{\partial t}. \quad (12)$$

Inserting Eq. (10) in the form $d\rho = \rho dh/c^2$ alongside the ambient enthalpy h_∞ into the continuity equation, Eq. (7), yields

$$\frac{1}{c^2} \frac{Dh}{Dt} + \nabla \cdot \mathbf{u} = \frac{1}{c^2} \frac{\partial h_\infty}{\partial t}. \quad (13)$$

For convenience, we also separate the kinetic energy and the rotation of the flow by reformulating the convective velocity derivative as

$$(\mathbf{u} \cdot \nabla) \mathbf{u} = \nabla \left(\frac{\mathbf{u}^2}{2} \right) - \mathbf{u} \times (\nabla \times \mathbf{u}), \quad (14)$$

with which the momentum equation, Eq. (8), becomes

$$\frac{\partial \mathbf{u}}{\partial t} + \nabla \left(\frac{\mathbf{u}^2}{2} \right) - \mathbf{u} \times (\nabla \times \mathbf{u}) + \nabla h = 0. \quad (15)$$

Note that, since the density and pressure have been replaced by the specific enthalpy and the speed of sound on the basis of the flow being isentropic, the entropy equation, Eq. (9), is now obsolete.

B. Hypothesis

The Kirkwood-Bethe hypothesis is typically derived and applied under the assumption of spherical symmetry. However, it can be derived more generally for one-dimensional problems, e.g. exploiting cylindrical symmetry⁶⁷, to explore the influence of the shape of a bubble on its dynamics and the induced flow field. Here, we consider an arbitrary (quasi) one-dimensional domain, illustrated in Figure 1, characterized by the dimensionality coefficient α that defines the effective dimensions of the system: $\alpha = 0$ describing a planar case, $\alpha = 1$ describing cylindrical symmetry, and $\alpha = 2$ describing the conventionally assumed spherical symmetry.

Considering a (quasi) one-dimensional flow by exploiting the symmetry of the system, we know that the flow is *irrotational*, with $\nabla \times \mathbf{u} = 0$. The continuity equation, Eq. (13), and the momentum equation, Eq. (15), along the one-dimensional spatial coordinate r are, therefore, given as

$$\frac{1}{c^2} \left(\frac{\partial h}{\partial t} + u \frac{\partial h}{\partial r} \right) + \frac{1}{r^\alpha} \frac{\partial}{\partial r} (r^\alpha u) = \frac{1}{c^2} \frac{\partial h_\infty}{\partial t} \quad (16)$$

$$\frac{\partial u}{\partial t} + \frac{\partial}{\partial r} \left(\frac{u^2}{2} \right) + \frac{\partial h}{\partial r} = 0. \quad (17)$$

Since the flow is irrotational, the velocity may be expressed in terms of the potential ψ ,

$$u = -\frac{\partial \psi}{\partial r}, \quad (18)$$

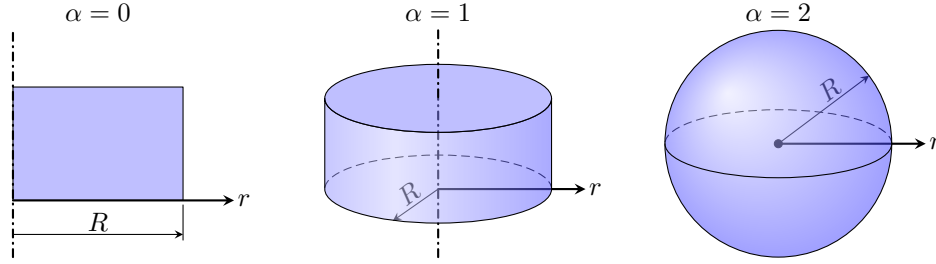


FIG. 1: Schematic illustration of the considered (quasi) one-dimensional domains: one-dimensional planar ($\alpha = 0$), cylindrical symmetry ($\alpha = 1$), and spherical symmetry ($\alpha = 2$). The one-dimensional spatial coordinate is denoted with r and the width or radius of the gas cavity or bubble is denoted with R .

with which the continuity and momentum equations can be written as

$$\frac{1}{c^2} \left(\frac{\partial h}{\partial t} - \frac{\partial h_\infty}{\partial t} + u \frac{\partial h}{\partial r} \right) - \frac{1}{r^\alpha} \frac{\partial}{\partial r} \left(r^\alpha \frac{\partial \psi}{\partial r} \right) = 0 \quad (19)$$

$$-\frac{\partial}{\partial t} \frac{\partial \psi}{\partial r} + \frac{\partial}{\partial r} \left(\frac{u^2}{2} \right) + \frac{\partial h}{\partial r} = 0. \quad (20)$$

Integrating Eq. (20) from r to ∞ , assuming the potential ψ vanishes at infinity, yields the transient Bernoulli equation,

$$-\frac{\partial \psi}{\partial t} + \frac{u^2}{2} + h - h_\infty = 0, \quad (21)$$

based on which Kirkwood and Bethe⁴³ defined the specific kinetic enthalpy as

$$\Omega = \frac{\partial \psi}{\partial t} = h - h_\infty + \frac{u^2}{2}. \quad (22)$$

Rearranging Eq. (22) for the enthalpy difference $h - h_\infty$ and inserting the resulting expression into the continuity equation, Eq. (19), yields

$$\frac{1}{c^2} \left(\frac{\partial^2 \psi}{\partial t^2} + u \frac{\partial}{\partial r} \frac{\partial \psi}{\partial t} - \frac{1}{2} \frac{\partial u^2}{\partial t} - \frac{1}{2} u \frac{\partial u^2}{\partial r} \right) - \frac{1}{r^\alpha} \frac{\partial}{\partial r} \left(r^\alpha \frac{\partial \psi}{\partial r} \right) = 0. \quad (23)$$

Noting that the last term on the left-hand side is the Laplacian of the velocity potential,

$$\nabla^2 \psi = \frac{1}{r^\alpha} \frac{\partial}{\partial r} \left(r^\alpha \frac{\partial \psi}{\partial r} \right), \quad (24)$$

Eq. (23) can be rewritten as a wave equation with a nonlinear correction of order $\mathcal{O}(u^2)$,^{43,175}

$$\frac{1}{c^2} \frac{\partial^2 \psi}{\partial t^2} - \nabla^2 \psi = \frac{1}{c^2} \left(\frac{\partial u^2}{\partial t} + \frac{1}{2} u \frac{\partial u^2}{\partial r} \right), \quad (25)$$

suggesting that the velocity potential ψ propagates like a wave. As discussed in detail by Prosperetti¹⁷⁶, the

finite propagation speed is unimportant in the near field, where the flow behaves similar to an incompressible fluid ($c \rightarrow \infty$), with $\nabla^2 \psi = 0$, while the perturbations are small in the far field, such that terms of order $\mathcal{O}(u^2)$ become negligible⁷⁹, and Eq. (25) reduces to the classic form of the wave equation,

$$\frac{1}{c^2} \frac{\partial^2 \psi}{\partial t^2} - \nabla^2 \psi = 0. \quad (26)$$

Comparing the magnitude of the right-hand side of Eq. (25) to the magnitude of the second-order time derivative of the velocity potential on the left-hand side may be used to quantify the local error of using a wave equation to propagate acoustic information in this case¹⁰⁵.

The work of Kirkwood and Bethe⁴³ rests on a reformulated velocity potential in spherical symmetry, defined as $\phi = r\psi$. With this new potential, the wave equation, Eq. (25), becomes

$$\frac{1}{c^2} \frac{\partial^2 \phi}{\partial t^2} - \frac{\partial^2 \phi}{\partial r^2} = \frac{r}{c^2} \left(\frac{\partial u^2}{\partial t} + \frac{1}{2} u \frac{\partial u^2}{\partial r} \right) \quad (27)$$

and the transient Bernoulli equation, Eq. (21), yields

$$\frac{\partial \phi}{\partial t} = r \frac{\partial \psi}{\partial t} = r \left(h - h_\infty + \frac{u^2}{2} \right), \quad (28)$$

which is, in fact, the quantity defined in Eq. (1). Adopting this principle for the general one-dimensional domain considered here, with α defining the symmetry of the problem, the reformulated velocity potential is defined as $\phi = r^{\alpha/2} \psi$, originally proposed by Rice and Ginell⁶⁷. The wave equation then reads as

$$\frac{1}{c^2} \frac{\partial^2 \phi}{\partial t^2} - \frac{\partial^2 \phi}{\partial r^2} = \frac{r^{\alpha/2}}{c^2} \left(\frac{\partial u^2}{\partial t} + \frac{1}{2} u \frac{\partial u^2}{\partial r} \right) \quad (29)$$

and the transient Bernoulli equation yields

$$\frac{\partial \phi}{\partial t} = r^{\alpha/2} \frac{\partial \psi}{\partial t} = r^{\alpha/2} \left(h - h_\infty + \frac{u^2}{2} \right). \quad (30)$$

The validity of this definition of the velocity potential is further discussed together with the limitations presented by the dimensionality coefficient α in Section III C.

In principle, the method of characteristics may be applied to solve the wave equation governing the velocity potential and any of its derivatives, even though an analytical solution is not readily obtainable due to the contributions of $\mathcal{O}(u^2)$.⁷⁹ The *Kirkwood-Bethe hypothesis* stipulates that the quantity $g = \partial\phi/\partial t$, as given by Eq. (30), is constant along an outgoing characteristic, satisfying⁴³

$$\left. \frac{dg}{dt} \right|_c = 0, \quad (31)$$

where the derivative operator along an outgoing characteristic is defined as

$$\left. \frac{d}{dt} \right|_c = \frac{\partial}{\partial t} + \left. \frac{dr}{dt} \right|_c \frac{\partial}{\partial r}. \quad (32)$$

Observing that small disturbances to the velocity potential of the fluid propagate like a wave according to Eq. (25), i.e. with speed c relative to the flow, Kirkwood and Bethe⁴³ proposed to approximate the propagation speed along an outgoing characteristic by

$$\left. \frac{dr}{dt} \right|_c = c + u. \quad (33)$$

C. Limitations

The assumption of a constant value of $g = r^{\alpha/2}(h - h_\infty + u^2/2)$ along outgoing characteristics can be justified by the conservation of specific energy when dissipative effects are neglected, as it follows from the transient Bernoulli equation. However, the assumptions that the acoustic potential is $\phi = r^{\alpha/2}\psi$ and propagates with speed $c + u$ may entail errors.

A plane finite-amplitude acoustic wave moving in one direction (*cf.* simple wave) propagates with speed $c + u$,¹⁷⁷ and $c \pm u$ are the eigenvalues of the Euler equations for plane waves,¹⁷⁸ meaning that plane waves travel with the local speed of sound c relative to the flow⁸⁷. Moreover, Eq. (33) reduces to the asymptotic speed c in the far field, since $u \rightarrow 0$ for $r \rightarrow \infty$, and is consistent with the Chapman-Jouguet condition^{179,180} for detonation waves. However, the propagation speed $c + u$ is not exact. This can be seen by considering the Riemann function ς for an isentropic flow¹⁸¹,

$$\varsigma = \int_{p_\infty}^p \frac{dp}{\rho c} = \int_{h_\infty}^h \frac{dh}{c}. \quad (34)$$

Introducing ς into the continuity and momentum equations, Eqs. (16) and (17), yields

$$\frac{\partial}{\partial t}(\varsigma + u) + (c + u) \frac{\partial}{\partial r}(\varsigma + u) = -\frac{\alpha u c}{r} \quad (35)$$

$$\frac{\partial}{\partial t}(\varsigma - u) + (c - u) \frac{\partial}{\partial r}(\varsigma - u) = -\frac{\alpha u c}{r}, \quad (36)$$

with the quantities $\varsigma + u$ and $\varsigma - u$ being so-called *Riemann invariants*¹⁸¹. For a plane wave ($\alpha = 0$), the Riemann invariant $\varsigma + u$ propagates with constant value along the right-going characteristic with speed $c + u$, whereas $\varsigma - u$ propagates with constant value along the left-going characteristic with speed $c - u$. When the right-hand side, which accounts for the geometric divergence of, for instance, cylindrical ($\alpha = 1$) or spherical ($\alpha = 2$) domains, is not zero, the Riemann invariants $\varsigma + u$ and $\varsigma - u$ do not propagate with $c + u$ and $c - u$, respectively. Hence, quantities that are invariant along outgoing characteristics of a curved wave do not propagate with speed $c + u$, rendering Eq. (33) an approximation that becomes more accurate as a curved wave moves outwards or when the velocity is small with respect to the speed of sound⁶². Assuming the (dominant) fluid flow is the result of the bubble motion and the associated acoustic emissions only, the velocity is $u \propto r^{-\alpha/2}$ in the far field and, hence, the right-hand side of Eq. (35) decays rapidly with r^{-n} , where $n \geq 1 + \alpha/2$.

Considering a plane acoustic wave, the acoustic particle velocity $u_1 = p_1/(\rho c)$ is in phase with the acoustic pressure p_1 , whereby p_1 and u_1 follow from the expansions $p = p_0 + p_1$ and $u = u_0 + u_1$, and where subscript 0 denotes the reference or ambient properties of the flow field. However, u_1 and p_1 of a curved wave are not in phase¹⁸². As a consequence, the specific acoustic impedance $z = p_1/u_1$ experienced by a curved wave is complex, given for a spherical harmonic wave as^{182,183}

$$z = \rho c \frac{(kr)^2 + ikr}{1 + (kr)^2}, \quad (37)$$

which is dependent on the wavenumber k and radial coordinate r , and where i denotes the imaginary unit. For large r , the imaginary part (specific acoustic reactance) vanishes and the real part (specific acoustic resistance) approaches the specific acoustic impedance of a plane wave, $z = \rho c$, whereas the imaginary part dominates for small r . KBH models do not account for this complex acoustic impedance and the associated error is investigated in Section IX B.

The dimensionality coefficient α defines the dimension and symmetry of the considered problem. Inserting $\phi = r^{\alpha/2}\psi$ in the corresponding wave equation, Eq. (29), reads as

$$\frac{1}{c^2} \frac{\partial^2(r^{\alpha/2}\psi)}{\partial t^2} - \frac{\partial^2(r^{\alpha/2}\psi)}{\partial r^2} = \frac{r^{\alpha/2}}{c^2} \left(\frac{\partial u^2}{\partial t} + \frac{1}{2} u \frac{\partial u^2}{\partial r} \right), \quad (38)$$

which, after expanding the left-hand side and dividing by $r^{\alpha/2}$, becomes

$$\begin{aligned} \frac{1}{c^2} \frac{\partial^2 \psi}{\partial t^2} - \underbrace{\left(\frac{\partial^2 \psi}{\partial r^2} + \frac{\alpha}{r} \frac{\partial \psi}{\partial r} \right)}_{\nabla^2 \psi, \text{ Eq. (24)}} - \frac{\alpha(\alpha - 2)}{4r^2} \psi \\ = \frac{1}{c^2} \left(\frac{\partial u^2}{\partial t} + \frac{1}{2} u \frac{\partial u^2}{\partial r} \right). \end{aligned} \quad (39)$$

The last term on the left-hand side vanishes for plane ($\alpha = 0$) and spherical ($\alpha = 2$) waves, such that Eq. (39) is identical to Eq. (25). This means that the potential ψ and the shape of plane and spherical waves of small amplitude, where $u^2 \ll c^2$, remain unchanged as they propagate away from the emitter. However, the corresponding wave equation for cylindrical waves ($\alpha = 1$),

$$\frac{1}{c^2} \frac{\partial^2 \psi}{\partial t^2} - \nabla^2 \psi + \frac{\psi}{4r^2} = \frac{1}{c^2} \left(\frac{\partial u^2}{\partial t} + \frac{1}{2} u \frac{\partial u^2}{\partial r} \right), \quad (40)$$

contains a spurious term proportional to $1/r^2$ and provides an accurate solution only in the asymptotic limit $r \rightarrow \infty$.^{67,184} In fact, in the interval $0 \leq \alpha \leq 2$, the spurious term in Eq. (39) is largest for $\alpha = 1$, and Rice and Ginell^{67,68} reported more accurate results for cylindrical underwater explosions with $\alpha = 0.8$.

In summary, the assumptions underpinning the Kirkwood-Bethe hypothesis are, strictly speaking, valid only when either the wavelength is relatively small, such that the plane wave assumption is valid¹⁸⁵, or when the Mach number of the induced flow is small. The various modelling errors of the Kirkwood-Bethe hypothesis vanish in the asymptotic limits $r \rightarrow \infty$, representing the far field, or $u \rightarrow 0$, representing the linear acoustic regime. More generally, the Kirkwood-Bethe hypothesis can be regarded as an extrapolation of the linear acoustic theory¹⁷⁶ and, as briefly revisited in Section VII, is part of a consistent hierarchy of models^{60,186}. Nevertheless, as further discussed in Section IX, the Kirkwood-Bethe hypothesis provides accurate predictions under the specific conditions associated with pressure-driven bubble dynamics, cavitation and underwater explosions.

IV. LIQUID EQUATION OF STATE

The Kirkwood-Bethe hypothesis does not assume a specific equation of state (EoS) for the liquid, even though it is almost always presented and used in conjunction with the modified Tait EoS⁸⁶, which Kirkwood and Bethe⁴³ used in their original work. Similarly, the influential works of Cole³¹ on underwater explosions and Gilmore⁶² on cavitation also used the modified Tait EoS. The reasons for the popularity of this EoS are rather straightforward: it has a simple analytical form and it provides an accurate (isentropic) relationship between the pressure p , the specific enthalpy h , the density ρ , and the speed of sound c of water, even when compared against modern standards, such as the IAPWS R6-95(2018) standard¹⁸⁷.

While the original Tait EoS is formulated along isotherms⁸⁶,

$$-\left(\frac{\partial v}{\partial p}\right)_T = \frac{1}{n[p + B(T)]}, \quad (41)$$

where $v = 1/\rho$ is the specific volume, n is the polytropic exponent, and B is a pressure constant, the modified Tait

EoS used widely in conjunction with the Kirkwood-Bethe hypothesis is formulated along isentropes³¹

$$-\frac{1}{v} \left(\frac{\partial v}{\partial p} \right)_s = \frac{1}{n[p + B(s)]}, \quad (42)$$

which is, in essence, the isentropic (or, more generally, polytropic) form of the stiffened-gas EoS^{188,189}. The modified Tait EoS defines the fluid properties based on the pressure p as

$$h = \frac{n}{n-1} \frac{p+B}{\rho} \quad (43)$$

$$\rho = \rho_0 \left(\frac{p+B}{p_0+B} \right)^{\frac{1}{n}} \quad (44)$$

$$c = \sqrt{n \frac{p+B}{\rho}}, \quad (45)$$

where subscript 0 defines a reference state. For water, commonly used values are $n \approx 7$ and $B \approx 3 \times 10^8$ Pa, or $B \approx \rho_0 c_0^2/n$.⁴³ The reference density, pressure and speed of sound of water are typically assumed to be $\rho_0 \approx 1000$ kg/m³, $p_0 \approx 10^5$ Pa, and $c_0 \approx 1500$ m/s, respectively. Figure 2 shows the density, speed of sound and temperature predicted by the Tait EoS in comparison to the IAPWS R6-95(2018) standard.

The polytropic exponent for an isentropic flow represents the ratio of specific heats, which is approximately unity for water and other liquids. Thus, the large polytropic exponent for water, $n \approx 7$, points to the main shortcoming of the Tait EoS: it severely overpredicts changes in temperature as a result of adiabatic compression or expansion^{89,90},

$$T = T_0 \left(\frac{p+B}{p_0+B} \right)^{(n-1)/n}, \quad (46)$$

as seen in Figure 2. In fact, during a violent bubble collapse, the Tait EoS may predict the temperature of the liquid in the vicinity of the gas-liquid interface to be higher than the temperature inside the gas bubble⁹⁰, which is unphysical on account of the considerably larger heat capacity of liquids compared to gases.

To rectify this shortcoming of the Tait EoS and, similarly, the stiffened-gas EoS, Le Métayer and Saurel⁸⁸ proposed the Noble-Abel stiffened-gas (NASG) EoS, which had already been postulated in similar (isothermal) form by Tammann¹⁹¹. The NASG EoS extends the Tait and stiffened-gas EoS by introducing the co-volume b that represents the finite volume occupied by the fluid molecules, rendering the NASG EoS a simplified version of the van-der-Waals EoS¹⁹² with constant coefficients B and b . For an isentropic flow the specific enthalpy, den-

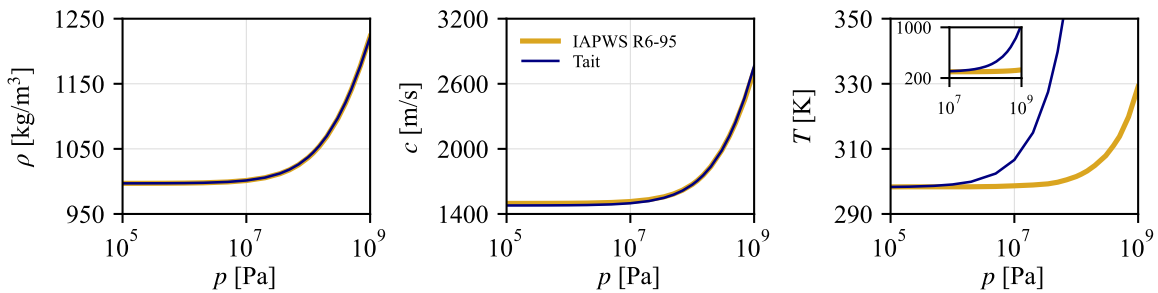


FIG. 2: Density ρ , speed of sound c , and temperature T of water obtained with the modified Tait EoS, using the model constants of Cole³¹ ($n = 7.15$ and $B = 3047 \times 10^5$ Pa), compared against the IAPWS R6-95(2018) standard. The reference values are $p_0 = 10^5$ Pa, $\rho_0 = 997$ kg/m³, and $T_0 = 298.3$ K.

TABLE I: Model constants of the NASG EoS for water proposed in recent years.

	Le Métayer and Saurel ⁸⁸	Chandran and Salih ¹⁹⁰	Denner and Schenke ⁶⁰
n	1.19	1.19	1.11
B [Pa]	7028×10^5	6218×10^5	6480×10^5
b [m ³ /kg]	6.61×10^{-4}	6.72×10^{-4}	6.80×10^{-4}
ρ_0 [kg/m ³]	957.7	997.0	997.0
p_0 [Pa]	1.0453×10^5	10^5	10^5

sity and speed of sound are defined as⁹⁰

$$h = \frac{n}{n-1} \frac{p+B}{\rho} - \frac{nb}{n-1} (p+B) + bp \quad (47)$$

$$\rho = \frac{K(p+B)^{\frac{1}{n}}}{1 + bK(p+B)^{\frac{1}{n}}} \quad (48)$$

$$c = \sqrt{n \frac{p+B}{\rho - b\rho^2}}, \quad (49)$$

where $K = \rho_0 / [(p_0 + B)^{1/n} (1 - b\rho_0)]$ describes a constant reference state. Just like the Tait EoS, to which it reduces for $b = 0$, the NASG EoS is unconditionally convex⁸⁸, making it an equally robust alternative to the Tait EoS. The temperature as a result of adiabatic compression and expansion is also for the NASG EoS given by Eq. (46). Different model constants for the NASG EoS of water have been proposed in recent years, as listed in Table I and shown in Figure 3. In particular the model constants for isentropic water proposed by Denner and Schenke⁶⁰ exhibit a very good agreement with the IAPWS R6-95(2018) standard. The NASG EoS was first used in conjunction with the Kirkwood-Bethe hypothesis in the Gilmore-NASG model for bubble dynamics by Denner⁹⁰ and, using the theory derived in Section VI for spherical bubbles, to model the full flow field introduced by cavitation bubbles by Denner and Schenke⁶⁰.

Other equations of state, such as the van-der-Waals EoS or any tabulated EoS, may also be applied in conjunction with the Kirkwood-Bethe hypothesis. However, the simplicity and robustness of the Tait EoS and, more recently, the NASG EoS have prevailed so far.

V. BUBBLE DYNAMICS

The propagation of the invariant g along outgoing characteristics, as stipulated by the Kirkwood-Bethe hypothesis, can be readily employed to derive the equation of motion of the gas-liquid interface of a gas bubble or cavity.

Expanding Eq. (31) under consideration of the time-dependent ambient enthalpy defined by Eq. (12) yields

$$r \frac{Dh}{Dt} - r \frac{Dh_\infty}{Dt} + ru \frac{Du}{Dt} + rc \left(\frac{\partial h}{\partial r} + u \frac{\partial u}{\partial r} \right) + \frac{\alpha}{2} \left(h - h_\infty + \frac{u^2}{2} \right) \frac{dr}{dt} \Big|_c = 0. \quad (50)$$

Expressions for the spatial derivatives of the flow velocity and specific enthalpy follow by rearranging the continuity and momentum equations, Eqs. (16) and (17), as

$$\frac{\partial u}{\partial r} = -\frac{1}{c^2} \left(\frac{Dh}{Dt} - \frac{Dh_\infty}{Dt} \right) - \frac{\alpha u}{r} \quad (51)$$

$$\frac{\partial h}{\partial r} = -\frac{Du}{Dt}, \quad (52)$$

respectively. Inserting Eqs. (33), (51), and (52) into Eq. (50), we obtain

$$r \left(\frac{Dh}{Dt} - \frac{Dh_\infty}{Dt} \right) + r \frac{Du}{Dt} (u - c) - \frac{ru}{c} \left(\frac{Dh}{Dt} - \frac{Dh_\infty}{Dt} \right) - \alpha cu^2 + \frac{\alpha}{2} \left(h - h_\infty + \frac{u^2}{2} \right) (c + u) = 0. \quad (53)$$

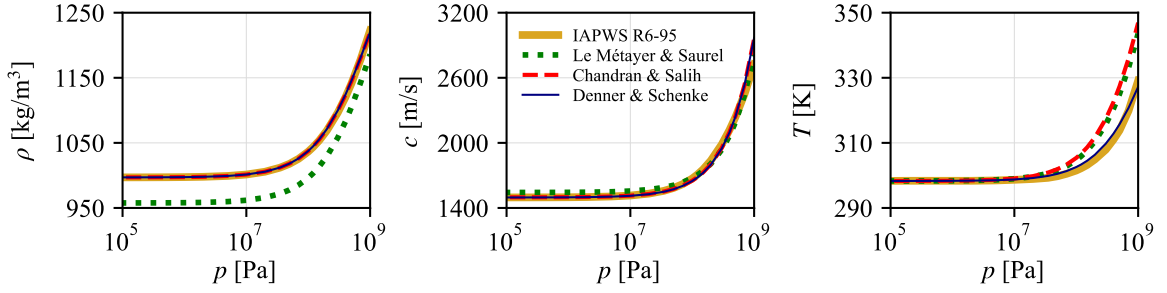


FIG. 3: Density ρ , speed of sound c , and temperature T of water obtained with the NASG EoS, using the model constants listed in Table I, compared against the IAPWS R6-95(2018) standard. The reference temperature is $T_0 = 298.3$ K.

Evaluating this equation at the gas-liquid interface ($r = R$) yields a second-order ODE describing the change in radius R of a gas bubble or cavity, given as

$$\begin{aligned} \left(1 - \frac{\dot{R}}{c_L}\right) R\ddot{R} + \frac{3}{4}\alpha \left(1 - \frac{\dot{R}}{3c_L}\right) \dot{R}^2 \\ = \frac{\alpha}{2} \left(1 + \frac{\dot{R}}{c_L}\right) H + \left(1 - \frac{\dot{R}}{c_L}\right) \frac{R\dot{H}}{c_L}, \end{aligned} \quad (54)$$

with $H = h_L - h_\infty$ and $\dot{H} = \dot{h}_L - \dot{h}_\infty$, where $\dot{\diamond} = D\diamond/Dt$ denotes the material derivative at the gas-liquid interface and the subscript L denotes quantities of the liquid at the gas-liquid interface. In this general form, Eq. (54) was first presented by Kedrinskii and Kuzavov⁸⁵, while in spherical symmetry ($\alpha = 2$), Eq. (54) is the well-known Gilmore equation⁶²

$$\begin{aligned} \left(1 - \frac{\dot{R}}{c_L}\right) R\ddot{R} + \frac{3}{2} \left(1 - \frac{\dot{R}}{3c_L}\right) \dot{R}^2 \\ = \left(1 + \frac{\dot{R}}{c_L}\right) H + \left(1 - \frac{\dot{R}}{c_L}\right) \frac{R\dot{H}}{c_L}. \end{aligned} \quad (55)$$

Note that the assumption of a cylindrical or spherical bubble, as well as the assumption of a spatially invariant ambient enthalpy h_∞ , are only valid if $\lambda_\infty \gg R$,^{193,194} where λ_∞ is the wavelength of $h_\infty(t)$.

The specific enthalpy h_L incorporates the kinematic boundary conditions at the gas-liquid interface. Considering a Newtonian liquid and a clean gas-liquid interface without surface-active substances, the liquid pressure p_L at the gas-liquid interface is defined as¹⁹⁵

$$p_L = p_G - \frac{\alpha\sigma}{R} - 2\alpha \frac{\mu\dot{R}}{R}, \quad (56)$$

where σ is the surface tension coefficient and μ is the dynamic viscosity of the liquid. The Gilmore model has also been used in conjunction with viscoelastic materials surrounding the gas bubble^{143,144,146,196} and considering a coated gas-liquid interface^{60,142–144}.

The gas pressure inside the bubble, p_G , is defined by an appropriate EoS as a function of the bubble size. Assuming the gas to be ideal, the pressure in the bubble to be spatially uniform and the compression to be adiabatic, the gas pressure of a cavitation bubble under consideration of the dimensionality parameter α is given as

$$p_G = p_{G,0} \left(\frac{R_0^{\alpha+1}}{R^{\alpha+1}}\right)^\gamma, \quad (57)$$

where $p_{G,0}$ is the gas pressure at initial radius R_0 and γ is the ratio of specific heats (or, more generally, the polytropic exponent) of the gas. The finite volume occupied by the gas molecules, which becomes important during a strong bubble collapse, can be taken into account by the van-der-Waals hardcore radius r_{hc} ,¹⁵⁷ such that

$$p_G = p_{G,0} \left(\frac{R_0^{\alpha+1} - r_{hc}^{\alpha+1}}{R^{\alpha+1} - r_{hc}^{\alpha+1}}\right)^\gamma. \quad (58)$$

Alternatively, the same can be achieved with the Noble-Abel (NA) EoS^{197,198}, a simplification of the NASG EoS discussed in Section IV, with which the gas pressure and density as a result of adiabatic compression are defined as⁹⁰

$$p_G = p_{G,0} \left[\frac{\rho_G(1 - b\rho_{G,0})}{\rho_{G,0}(1 - b\rho_G)}\right]^\gamma \quad (59)$$

$$\rho_G = \rho_{G,0} \left(\frac{R_0}{R}\right)^{\alpha+1}, \quad (60)$$

respectively, where $\rho_{G,0}$ is the gas density at pressure $p_{G,0}$ and b is the co-volume of the gas. More elaborate gas models that dispense with the polytropic relation or use more complex gas equations of state^{199–201}, account for heat transfer^{202–206}, mass transfer^{34,124,200,201,206}, and external damping effects³⁴ can also be readily applied in conjunction with the Gilmore model. For underwater explosions, the Jones-Wilkins-Lee (JWL) EoS^{207,208} is a popular choice in conjunction with the Chapman-Jouguet isentrope^{179,180} to describe the properties of the gaseous detonation products constituting the bubble and to provide initial conditions for the velocity of the gas-liquid interface^{98,100–102,104,209–211}.

The Gilmore equation for spherical bubbles, Eq. (55), has been shown in many studies to yield remarkably accurate results, which Prosperetti and Lezzi^{212,213} attributed to the fact that the specific enthalpy of the liquid is retained in the equation of motion. Even though the Gilmore equation contains some high-order terms, it is not consistently second-order accurate with respect to the Mach number of the gas-liquid interface. Benjamin²¹⁴ pointed to missing second-order terms in the Kirkwood-Bethe hypothesis, which was met with some skepticism by Plesset (see the discussion on p. 232-233 in the book edited by Cooper⁷²), although similar second-order errors in the Gilmore model⁶² were later identified by Tilmann¹⁹⁴ and Prosperetti and Lezzi²¹². Lezzi and Prosperetti²¹³ proposed a more elaborate equation of motion for pressure-driven dynamics of spherical bubbles that is second-order accurate with respect to the Mach number, which was, however, derived under the explicit assumption that the velocity of the induced flow is small. Recent studies^{98,101,104} have used the model of Lezzi and Prosperetti²¹³ in conjunction with the Kirkwood-Bethe hypothesis successfully to predict the pressure transients and shock waves generated by underwater explosions.

VI. FLOW FIELD AROUND A BUBBLE

The flow field generated by an oscillating or collapsing bubble, or an underwater explosion, can be predicted with expressions derived from the Kirkwood-Bethe hypothesis in conjunction with the appropriate conservation laws. To this end, the original work of Kirkwood and Bethe⁴³, as well as subsequent studies by Rice and Ginell^{67,68}, Akulichev *et al.*⁷⁹, and Kedrinskii⁸⁰ focused on deriving models for the evolution of the peak pressure of a shock wave emitted by an underwater explosion or a pressure-driven bubble, leveraging the Kirkwood-Bethe hypothesis together with the Rankine-Hugoniot conditions. Since the Rankine-Hugoniot conditions follow from the governing conservation laws at shock discontinuities, these peak-pressure models can be seen a special case of the more general descriptions of the flow field devised by Gilmore⁶², Hickling and Plesset⁶⁴, and Ivany⁴⁴.

The enthalpy of the fluid is readily obtained by rearranging Eq. (30) as

$$h = h_\infty + \frac{g}{r^{\alpha/2}} - \frac{u^2}{2}, \quad (61)$$

where the invariant g is defined by Eq. (30), using the conditions under which it originates at the gas-liquid interface ($R = r$), as

$$g = R^{\alpha/2} \Omega_L = R^{\alpha/2} \left(h_L - h_\infty + \frac{\dot{R}^2}{2} \right). \quad (62)$$

Inserting Eq. (62) into Eq. (61), the specific enthalpy at

radial location r and time t is

$$h(r, t) = h_\infty(t) + \left[\frac{R(\tau)}{r(t)} \right]^{\alpha/2} \Omega_L(\tau) - \frac{u(r, t)^2}{2}, \quad (63)$$

where $\tau = t - r/(c + u)$ is the retarded time that corresponds to the time at which the invariant g or, likewise, the specific kinetic enthalpy Ω are emitted at the gas-liquid interface. This definition of the specific enthalpy satisfies the boundary condition $h(R, \tau) = h_L(\tau)$ at the gas-liquid interface ($r = R$). Considering, in addition, that h_∞ is an explicitly imposed ambient enthalpy and the radial position r can be obtained by integrating Eq. (33), the flow velocity u is the only remaining unknown.

Eqs. (33) and (63), in conjunction with either the explicit expression, Eq. (69), or the differential equation, Eq. (75), for the flow velocity derived below, describe the flow field induced by a bubble or cavity with varying size, assuming the induced flow is isentropic.

A. Explicit expression for the flow velocity

By directly inserting the velocity potential $\psi = \phi/r^{\alpha/2}$ into the definition of the velocity given by Eq. (18), similar to the derivation of the quasi-acoustic description of the flow field presented by Gilmore⁶² and Trilling⁸⁴, we obtain

$$u = \frac{\alpha \phi}{2 r^{1+\alpha/2}} - \frac{1}{r^{\alpha/2}} \frac{\partial \phi}{\partial r}. \quad (64)$$

Making the assumption that the potential ϕ propagates with constant value along outgoing characteristics,

$$\left. \frac{d\phi}{dt} \right|_c = \left. \frac{\partial \phi}{\partial t} + \frac{dr}{dt} \right|_c \frac{\partial \phi}{\partial r} = 0, \quad (65)$$

allows us to write

$$\frac{\partial \phi}{\partial r} = - \left. \frac{dr}{dt} \right|_c^{-1} \frac{\partial \phi}{\partial t}. \quad (66)$$

Inserting this expression into Eq. (64) with the propagation velocity given by Eq. (33) and $g = \partial \phi / \partial t$, the flow velocity is defined as

$$u = \frac{\alpha \phi}{2 r^{1+\alpha/2}} + \frac{g}{r^{\alpha/2}(c + u)}. \quad (67)$$

This explicit expression of the flow velocity can already be found in the original report of Kirkwood and Bethe⁴³ for spherical symmetry ($\alpha = 2$) as well as in the report of Rice and Ginell⁶⁸ for cylindrical symmetry ($\alpha = 1$). Evaluating Eq. (67) at the gas-liquid interface ($R = r$), we find the invariant potential ϕ to be defined as

$$\phi = \frac{2}{\alpha} \left(R^{1+\alpha/2} \dot{R} - R \frac{g}{c_L + \dot{R}} \right). \quad (68)$$

Inserting Eqs. (62) and (68) into Eq. (67), the velocity at radial location r and time t is

$$u(r, t) = \left[\frac{R(\tau)}{r(t)} \right]^{1+\alpha/2} \left[\dot{R}(\tau) - \frac{\Omega_L(\tau)}{c_L(\tau) + \dot{R}(\tau)} \right] + \left[\frac{R(\tau)}{r(t)} \right]^{\alpha/2} \frac{\Omega_L(\tau)}{c(r, t) + u(r, t)}, \quad (69)$$

which satisfies the boundary condition $u(R, \tau) = \dot{R}(\tau)$ at the gas-liquid interface ($r = R$).

The explicit expression of the velocity given by Eq. (69) separates the flow velocity into three distinct contributions⁶⁰: the first term is the incompressible displacement of the fluid by the moving gas-liquid interface, the second term represents the compression/expansion of the fluid resulting from its displacement, and the third term is the particle velocity associated with the emitted acoustic wave. Hence, the first two terms represent hydrodynamic contributions and the third term represents the acoustic contribution to the flow field. However, the assumption that the potential ϕ propagates as an outgoing wave with constant amplitude is valid only if the nonlinear terms on the right-hand side of Eq. (29) are negligible. Hence, Eq. (67) is accurate only if the flow velocity is sufficiently small, $u^2 \ll c^2$.

B. Differential equation for the flow velocity

Alternative to the explicit expression for the flow velocity presented in the previous section, it is also possible to derive an ODE describing the flow velocity, as proposed by Gilmore⁶² and Hickling and Plesset⁶⁴, without the assumption that ϕ retains a constant value as it propagates outward. To this end, the continuity equation, Eq. (16), is added to the momentum equation, Eq. (17), to obtain

$$\frac{1}{c} \left(\frac{\partial h}{\partial t} + u \frac{\partial h}{\partial r} \right) + c \frac{\partial u}{\partial r} + \frac{\alpha u c}{r} + \frac{\partial u}{\partial t} + u \frac{\partial u}{\partial r} + \frac{\partial h}{\partial r} = \frac{1}{c} \frac{\partial h_\infty}{\partial t}. \quad (70)$$

This equation may be rearranged as

$$\frac{1}{c} \left[\frac{\partial h}{\partial t} + (c + u) \frac{\partial h}{\partial r} \right] + \frac{\partial u}{\partial t} + (c + u) \frac{\partial u}{\partial r} = -\frac{\alpha u c}{r} + \frac{1}{c} \frac{\partial h_\infty}{\partial t}, \quad (71)$$

which is, considering that the ambient specific enthalpy h_∞ is assumed to be spatially invariant, equivalent to the equation for the outgoing Riemann invariant, see Eq. (35). Thus, the derivation of a differential equation for the flow velocity starts from the equation governing a curved Riemann wave in an isentropic flow. This further shows that the propagation speed $c + u$, albeit only

approximately accurate, is inferred by the governing conservation laws.

The enthalpy derivative along outgoing characteristics follows from Eq. (71) as

$$\frac{dh}{dt} \Big|_c = -c \frac{du}{dt} \Big|_c - \frac{\alpha u c^2}{r} + \frac{\partial h_\infty}{\partial t}. \quad (72)$$

Taking the derivative of Eq. (30) along an outgoing characteristic reads as

$$\frac{dg}{dt} \Big|_c = \frac{\alpha g}{2r} \frac{dr}{dt} \Big|_c + r^{\alpha/2} \frac{dh}{dt} \Big|_c - r^{\alpha/2} \frac{dh_\infty}{dt} \Big|_c + r^{\alpha/2} u \frac{du}{dt} \Big|_c = 0, \quad (73)$$

where $(dg/dt)_c = 0$ by virtue of the Kirkwood-Bethe hypothesis, and $(dh_\infty/dt)_c = \partial h_\infty / \partial t$, since h_∞ is spatially invariant by definition. Inserting Eq. (73) into Eq. (72),

$$\frac{\partial h_\infty}{\partial t} - \frac{\alpha g}{2r^{(1+\alpha/2)}} \frac{dr}{dt} \Big|_c - u \frac{du}{dt} \Big|_c = -c \frac{du}{dt} \Big|_c - \frac{\alpha u c^2}{r} + \frac{\partial h_\infty}{\partial t}, \quad (74)$$

the derivative of the flow velocity u along an outgoing characteristic is given as

$$\frac{du}{dt} \Big|_c = \frac{\alpha}{r(c-u)} \left[\frac{g}{2r^{\alpha/2}} \frac{dr}{dt} \Big|_c - u c^2 \right], \quad (75)$$

or, by inserting Eq. (33),

$$\frac{du}{dt} \Big|_c = \frac{\alpha}{r(c-u)} \left[\frac{g}{2r^{\alpha/2}} (c+u) - u c^2 \right]. \quad (76)$$

In spherical symmetry ($\alpha = 2$), Eq. (76) corresponds to the ODE first presented by Hickling and Plesset⁶⁴,

$$\frac{du}{dt} \Big|_c = \frac{1}{r(c-u)} \left[\frac{g}{r} (c+u) - 2u c^2 \right]. \quad (77)$$

The derivation of this ODE for the flow velocity in the way presented here follows the derivation presented for the special case of spherical symmetry ($\alpha = 2$) by Ivany⁴⁴.

An ODE for the flow velocity with respect to the radial coordinate may be obtained by dividing Eq. (76) by Eq. (33),

$$\frac{du}{dr} \Big|_c = \frac{du}{dt} \Big|_c \frac{dr}{dt} \Big|_c^{-1} = \frac{\alpha}{r(c-u)} \left[\frac{g}{2r^{\alpha/2}} - \frac{u c^2}{c+u} \right], \quad (78)$$

an ODE first proposed by Gilmore⁶² for spherical symmetry ($\alpha = 2$) using the modified Tait EoS.

C. Liquid pressure

With an EoS for the liquid at hand, the pressure of the liquid can be computed based on the specific enthalpy h . Using the modified Tait EoS, the pressure of the liquid follows by inserting Eq. (44) into Eq. (43) to obtain

$$p = \left[\frac{(n-1)\rho_0}{n(p_0+B)^{1/n}} h \right]^{\frac{1}{1-1/n}} - B \quad (79)$$

or, using Eqs. (43) and (61), the pressure can be computed based on the invariant g ,

$$p = \rho \left[\frac{p_\infty + B}{\rho_\infty} + \frac{n-1}{n} \left(\frac{g}{r^{\alpha/2}} - \frac{u^2}{2} \right) \right] - B, \quad (80)$$

as introduced for spherical symmetry ($\alpha = 2$) by Ivany⁴⁴ and, later, Ebeling⁸¹. The pressure amplitude $\Delta p = p - p_\infty$ is dominated by the term $g/r^{\alpha/2}$, especially in the far field where $u \rightarrow 0$, thus recovering the well-known amplitude decay with $1/r$ in spherical symmetry ($\alpha = 2$) and $1/\sqrt{r}$ in cylindrical symmetry ($\alpha = 1$).⁸⁷ With the NASG EoS, the liquid pressure follows from Eqs. (47) and (61) in a similar manner as

$$p = \frac{(n-1)\rho h - (1-b\rho)nB}{n-b\rho}. \quad (81)$$

Since p and ρ depend explicitly on each other, Eqs. (80) and (81) may require an iterative evaluation⁶⁰, in order to reach a desired accuracy.

Alternatively, inserting Eq. (76) into Eq. (73), and rearranging for the enthalpy derivative yields

$$\left. \frac{dh}{dt} \right|_c = \frac{\alpha}{r(c-u)} \left[u^2 c^2 - \frac{g}{2r^{\alpha/2}}(c+u)c \right] + \frac{\partial h_\infty}{\partial t}. \quad (82)$$

By applying Eq. (10), the ODE for the pressure along outgoing characteristics follows as

$$\left. \frac{dp}{dt} \right|_c = \frac{\rho\alpha}{r(c-u)} \left[u^2 c^2 - \frac{g}{2r^{\alpha/2}}(c+u)c \right] + \frac{\partial p_\infty}{\partial t}, \quad (83)$$

which may be solved together with the ODEs for the radial position, Eq. (33), and the velocity, Eq. (76). Assuming spherical symmetry in conjunction with the modified Tait EoS, and neglecting ambient pressure changes, Eq. (83) simplifies to

$$\left. \frac{dp}{dt} \right|_c = \frac{\rho_0}{r(c-u)} \left(\frac{p+B}{p_0+B} \right)^{1/n} \left[2u^2 c^2 - \frac{g}{r}(c+u)c \right], \quad (84)$$

which has been used frequently instead of Eq. (80).

VII. MODEL HIERARCHY

KBH models for pressure-driven bubble dynamics and acoustics are part of a consistent hierarchy of

models^{60,71,176,186} that can be established by successive simplifications of the Kirkwood-Bethe hypothesis.

Assuming $u^2 \ll c_0^2$ and constant fluid properties ($\rho = \rho_0$, $c = c_0$), such that the EoS of the liquid becomes obsolete, the potential $\psi = \phi/r^{\alpha/2}$ is governed by the wave equation

$$\frac{1}{c_0^2} \frac{\partial^2 \psi}{\partial t^2} - \nabla^2 \psi = 0, \quad (85)$$

the propagation speed along outgoing characteristics is constant,

$$\left. \frac{dr}{dt} \right|_c = c_0, \quad (86)$$

and the specific enthalpy is defined by the first-order approximation $h = p/\rho_0$. The pressure, consequently, follows from Eq. (61) as

$$p = p_\infty + \rho_0 \left(\frac{g}{r^{\alpha/2}} - \frac{u^2}{2} \right), \quad (87)$$

which neglects terms proportional to c_0^{-2} and higher. Considering Eq. (86), the explicit expression for the flow velocity, Eq. (67), simplifies to

$$u = \frac{\alpha \phi}{2r^{1+\alpha/2}} + \frac{g}{r^{\alpha/2}c_0}. \quad (88)$$

Based on Eqs. (87) and (88), the invariants g and ϕ are defined at the gas-liquid interface ($r = R$), such that the boundary conditions are satisfied, as

$$g = R^{\alpha/2} \left(\frac{p_L - p_\infty}{\rho_0} + \frac{\dot{R}^2}{2} \right) \quad (89)$$

$$\phi = \frac{2}{\alpha} \left(R^{1+\alpha/2} \dot{R} - R \frac{g}{c_0} \right). \quad (90)$$

This presents, in fact, the quasi-acoustic model of Gilmore⁶² and Trilling⁸⁴, generalized with respect to the dimensionality coefficient α . Although this quasi-acoustic model incorporates a finite wave speed, it cannot describe the nonlinear distortion of acoustic waves and the formation of shock fronts, since all parts of a wave propagate with the same constant speed c_0 . Applying the same simplifications to the ODE for the radial bubble dynamics, Eq. (54), and neglecting the term proportional to c_0^{-2} , yields a generalized form of the Keller-Miksis equation,²¹⁵

$$\begin{aligned} & \left(1 - \frac{\dot{R}}{c_0} \right) R \ddot{R} + \frac{3}{4} \alpha \left(1 - \frac{\dot{R}}{3c_0} \right) \dot{R}^2 \\ & = \frac{\alpha}{2} \left(1 + \frac{\dot{R}}{c_0} \right) \frac{p_L - p_\infty}{\rho_0} + R \frac{\dot{p}_L - \dot{p}_\infty}{\rho_0 c_0}. \end{aligned} \quad (91)$$

The quasi-acoustic model and the Keller-Miksis equation are first-order accurate with respect to the Mach number and, thus, limited to small Mach numbers, $(\dot{R}/c_0)^2 \ll 1$.

Going one step further by assuming the fluid is incompressible, with $c_0 \rightarrow \infty$, the velocity potential is governed by $\nabla^2 \psi = 0$ and the propagation speed along outgoing characteristics is infinite. The pressure in the liquid is given by Eq. (87) and the flow velocity follows from Eq. (88) as

$$u = \left(\frac{R}{r}\right)^{1+\alpha/2} \dot{R}. \quad (92)$$

With $c_0 \rightarrow \infty$, the ODE for the radial bubble dynamics, Eq. (91), further reduces to a generalized form of the Rayleigh-Plesset equation^{1,195,216},

$$R\ddot{R} + \frac{3}{4}\alpha\dot{R}^2 = \frac{\alpha(p_L - p_\infty)}{2\rho_0}. \quad (93)$$

VIII. SOLUTION METHODS

The equations governing the bubble dynamics and the equations describing the flow field can be solved independent of each other. From the viewpoint of the bubble dynamics, this is possible because the Kirkwood-Bethe hypothesis connects the kinematic conditions at the gas-liquid interface to the spatially invariant ambient condition at an assumed infinite distance. The flow field, in turn, is defined by discrete pieces of information that evolve along a single spatial dimension with speed $c + u$ and are connected to their initial conditions originating at the gas-liquid interface by the invariant g . The solution methods presented in this section are implemented in the open-source software library APECSS¹⁹⁶.

A. Bubble dynamics

In order to solve the equation of motion of the gas-liquid interface, Eq. (54), we require expressions for the specific enthalpy difference H and its derivative \dot{H} . The specific enthalpy difference can be computed using a suitable EoS in conjunction with the liquid pressure at the gas-liquid interface p_L and the ambient pressure p_∞ .

Considering a Newtonian liquid, p_L is given by Eq. (56). Since $dh = dp/\rho$ for the considered isentropic flow, the derivative of the specific enthalpy difference is defined as

$$\begin{aligned} \dot{H} = \frac{\dot{p}_L}{\rho_L} - \frac{\dot{p}_\infty}{\rho_\infty} = \frac{1}{\rho_L} \left(\dot{p}_G + \frac{\alpha\sigma}{R^2} \dot{R} \right. \\ \left. + 2\alpha\mu \frac{\dot{R}^2}{R^2} - 2\alpha\mu \frac{\ddot{R}}{R} \right) - \frac{\dot{p}_\infty}{\rho_\infty}. \end{aligned} \quad (94)$$

Inserting Eq. (94) into Eq. (54) and gathering the \ddot{R} -

terms on the left-hand side yields

$$\begin{aligned} \left(c_L R + \frac{2\alpha\mu}{\rho_L} \right) \ddot{R} = \frac{\alpha}{2} \left(\frac{c_L + \dot{R}}{c_L - \dot{R}} H - \frac{3c_L - \dot{R}}{c_L - \dot{R}} \frac{\dot{R}^2}{2} \right) + \\ \frac{R}{\rho_L} \left(\dot{p}_G + \frac{\alpha\sigma}{R^2} \dot{R} + 2\alpha\mu \frac{\dot{R}^2}{R^2} \right) - \frac{R\dot{p}_\infty}{\rho_\infty}. \end{aligned} \quad (95)$$

We can solve this second-order ODE by separating it into two first-order ODEs for \dot{R} and $\dot{U} = \dot{R}$, such that at each time instance t_j we integrate the equations

$$\dot{R}_{j+1} = U_j \quad (96)$$

and

$$\begin{aligned} \dot{U}_{j+1} = \frac{\alpha}{2\mathcal{A}_j} \left(\frac{c_{L,j} + \dot{R}_j}{c_{L,j} - \dot{R}_j} H_j - \frac{3c_{L,j} - \dot{R}_j}{c_{L,j} - \dot{R}_j} \frac{\dot{R}_j^2}{2} \right) \\ + \frac{R_j}{\mathcal{A}_j} \left(\frac{\dot{p}_{G,j}}{\rho_{L,j}} + \frac{\alpha\sigma\dot{R}_j}{R_j^2\rho_{L,j}} + \frac{2\alpha\mu\dot{R}_j^2}{R_j^2\rho_{L,j}} - \frac{\dot{p}_{\infty,j}}{\rho_{\infty,j}} \right), \end{aligned} \quad (97)$$

where

$$\mathcal{A}_j = c_{L,j} R_j + \frac{2\alpha\mu}{\rho_{L,j}}. \quad (98)$$

The embedded fifth-order Runge-Kutta scheme of Dormand and Prince²¹⁷, which adapts the numerical time step $\Delta t_j = t_j - t_{j-1}$ based on the estimated solution error, is a common choice to integrate this system of ODEs, as it is, for instance, the basis of the `ode45` function in Matlab, the default solver of the `solve_ivp` function of the SciPy package, and used in the solver of the open-source cavitation software library APECSS¹⁹⁶.

B. Flow field

To solve the flow velocity and specific enthalpy (or pressure), the information originating at the gas-liquid interface is tracked along the outgoing characteristics, whereby each parcel of information propagates on its own characteristic with velocity $c + u$. To this end, the bubble radius R_j , the speed of the gas-liquid interface \dot{R}_j , and the specific enthalpy of the liquid at the gas-liquid interface $h_{L,j}$ obtained by solving Eqs. (96) and (97) serve as the initial conditions.

The invariant g of information parcel i is defined upon emission at the gas-liquid interface, at emission time τ_i , as

$$g_i = R(\tau_i)^{\alpha/2} \left[h_L(\tau_i) - h_\infty(\tau_i) + \frac{\dot{R}(\tau_i)^2}{2} \right]. \quad (99)$$

The radial position $r_{i,j}$ and flow velocity $u_{i,j}$ of each information parcel i at time t_j result from Eqs. (33) and (75), by integrating

$$\frac{dr}{dt} \Big|_{c(i,j)} = c_{i,j} + u_{i,j} \quad (100)$$

$$\left. \frac{du}{dt} \right|_{c(i,j)} = \frac{\alpha}{r_{i,j}(c_{i,j} - u_{i,j})} \left[\frac{g_i}{2r_{i,j}^{\alpha/2}} \left. \frac{dr}{dt} \right|_{c(i,j)} - u_{i,j} c_{i,j}^2 \right] \quad (101)$$

using a suitable integration scheme for ODEs together with the initial conditions $R(\tau_i)$ and $\dot{R}(\tau_i)$. Once the new radial position $r_{i,j}$ and flow velocity $u_{i,j}$ of information parcel i are determined, its specific enthalpy is readily given by Eq. (61) as

$$h_{i,j} = h_{\infty,j} + \frac{g_i}{r_{i,j}^{\alpha/2}} - \frac{u_{i,j}^2}{2}, \quad (102)$$

from which the local pressure and speed of sound can be computed using the employed EoS.

As an alternative to integrating the velocity using Eq. (101), although not used for the results presented in Section IX, the flow velocity may also be determined explicitly using Eq. (69), such that

$$u_{i,j} = \frac{\alpha \phi_i}{2r_{i,j}^{1+\alpha/2}} + \frac{g_i}{r_{i,j}^{\alpha/2}(c_{i,j} + u_{i,j})}, \quad (103)$$

with

$$\phi_i = \frac{2}{\alpha} \left[R(\tau_i)^{1+\alpha/2} \dot{R}(\tau_i) - R(\tau_i) \frac{g_i}{c_L(\tau_i) + \dot{R}(\tau_i)} \right] \quad (104)$$

if sufficiently small flow velocities are expected.

Ivany⁴⁴ proposed to solve the flow velocity and pressure along outgoing characteristics originating at the gas-liquid interface at selected time instances, after the solution of the bubble dynamics had been fully obtained. Denner and Schenke⁶⁰ presented a Lagrangian wave tracking algorithm, whereby the flow field is solved together with the bubble dynamics and the information originating from the gas-liquid interface is tracked along outgoing characteristics. To this end, Eqs. (100) and (101) are integrated together as a coupled system of ODEs by a conventional fourth-order Runge-Kutta scheme, using the same time step Δt_j as for the integration of Eqs. (96) and (97)¹⁹⁶.

C. Shock fronts

Because both the particle velocity and the speed of sound are monotone-increasing functions of the pressure^{218,219}, the parts of an acoustic wave with a higher pressure propagate faster than the parts of the same wave with a lower pressure. This pressure dependency of the propagation speed drives a progressive steepening of the emitted waves and, eventually, may lead to the formation of a shock front for waves with sufficiently large initial amplitude. These cumulative nonlinear effects may become dominant for $Mkr \gtrsim 1$, where k is the wavenumber of the emitted wave, irrespective of the Mach number M ;²²⁰ in the absence of dissipation, any

plane wave forms a shock wave in finite time. At the shock front, a frequency-dependent attenuation prevents fluid particles from overtaking the shock front²¹⁸ and, as postulated by Rudnick²²¹, the stabilization of the shock front is independent of the origin of the acting dissipation process, such as viscous stresses or thermal conduction. This can be observed in numerical simulations, where a stable shock front can form even in inviscid and non-conducting flows, if sufficient numerical dissipation is present^{178,222,223}.

When solving the flow field by propagating the relevant information along outgoing characteristics using a KBH model, the formation of a shock front is signified by the intersection of characteristics, as seen in Figure 4(a). This intersection of characteristics yields a multivalued solution, shown in Figure 4(b), that is not physical. Akulich *et al.*⁷⁹ applied the *rule of equal areas*⁸⁷ to post process the multivalued solutions resulting from intersecting characteristics. Taking a multivalued density profile as shown in Figure 4(b), the corresponding weak solution is obtained graphically by eliminating the multivalued solution in such a way, that the area under the curve remains unchanged, as illustrated in Figure 4(c). Thus, the integral of the multivalued solution and the integral of the discontinuous weak solution of the density profile are the same, such that mass is conserved²²⁴. This implies that the wave on either side of the shock front remains a simple wave traveling in one direction, without reflections introduced at the discontinuity²²⁰. This method has been used, for instance, in studies on laser-induced cavitation^{58,59,61,123} and sonoluminescence¹⁶³ to model the formation and attenuation of shock waves using the Kirkwood-Bethe hypothesis.

Utilizing the Lagrangian wave tracking algorithm mentioned in the previous section, Denner and Schenke⁶⁰ proposed to simply discard any information that overtakes the information propagating ahead of it, as illustrated in Figure 5, to account for the formation of shock fronts and the associated dissipation. Naugol'nykh²²⁰ described a similar procedure as ‘‘clipping of the vertices of its profile’’ when referring to the decay of plane sawtooth waves. This rather simple procedure aims to exploit the argument of Rudnick²²¹ that the stabilization of the shock front is independent of the origin of dissipation. However, even though the results obtained with this method are in reasonably good agreement with the result obtained by applying the rule of equal areas for shock waves produced by collapsing bubbles⁶⁰, discarding information by clipping the density profile does not redistribute mass. Hence, this simple shock treatment yields an error in mass conservation and overpredicts the attenuation of the shock front, as observed in Figure 4(c).

IX. FURTHER INVESTIGATION

KBH models have been tested and validated extensively^{58,60,61,101–104,125,126,129}, utilizing high-fidelity

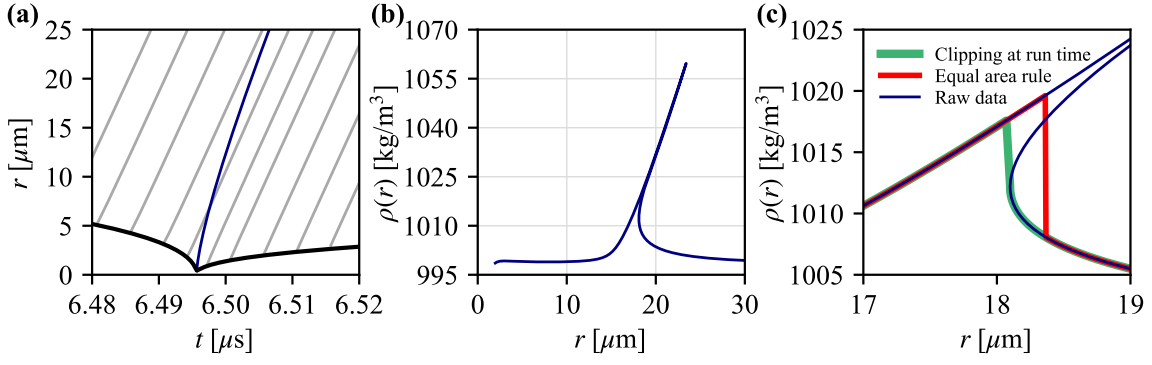


FIG. 4: Example of the different treatments of a shock front forming after the collapse of a cavitation bubble produced by a femtosecond laser, as studied by Liang *et al.*⁵⁹. (a) Selected outgoing wave characteristics are shown in a time-space plot, where the characteristic associated with the minimum radius is seen to intersect previously emitted characteristics. The thick black line shows the bubble radius. (b) The resulting multivalued density profile 50 ns after the bubble attained its minimum radius. (c) Close up of the density profile, to which two different shock treatments are applied. The clipping of the profile as proposed by Denner and Schenke⁶⁰ is applied at run time, whereas the rule of equal areas⁸⁷ is applied as a post-processing step.

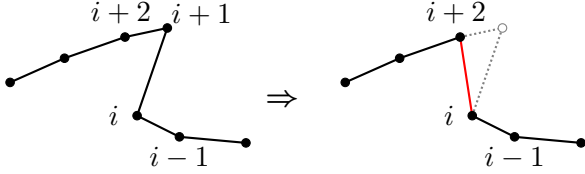


FIG. 5: Sketch of a discrete wave profile (left) with a multivalued solution and (right) after treating this multivalued solution by *clipping* the wave profile, as proposed by Denner and Schenke⁶⁰.

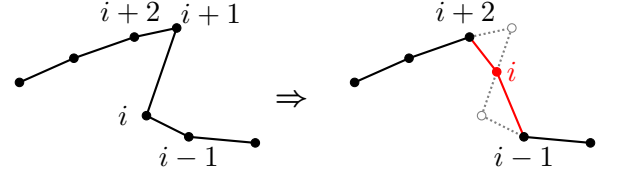


FIG. 6: Sketch of a discrete wave profile (left) with a multivalued solution and (right) after treating this multivalued solution by the proposed *averaging* procedure, Eqs. (105)-(107).

experiments and fully resolved simulations, and have been found to produce accurate and reliable results in a variety of scenarios. However, some fundamental questions regarding the validity and applicability of the Kirkwood-Bethe hypothesis remain. To further scrutinize and improve KBH models, this section focuses on the prediction of the propagation and attenuation of shock fronts at simulation run time (Section IX A) and the complex impedance of curved acoustic waves (Section IX B). The presented results were produced with version v1.6 of the open-source software library APECSS¹⁹⁶, available at <https://doi.org/10.5281/zenodo.10981878>.

A. Predicting shock fronts at simulation run time

The robust and accurate treatment of multivalued solutions associated with shock fronts at simulation run time presents challenges. Firstly, the full wave profile is required for an accurate treatment of a multivalued solution. This can be addressed when solving the flow along the outgoing characteristics by reconstructing the pressure or density profile in space. Secondly, however,

the multivalued solution should also be appropriately resolved in space. Assuming that we follow the discrete pieces of information that originate at the gas-liquid interface along the outgoing characteristic, e.g. as described in Section VIII B, the spatial resolution of the wave profile is directly dependent on the time step applied to solve the bubble dynamics.

While the application of the rule of equal areas provides an accurate means to rectify multivalued solutions, it is usually applied as a post-processing step. The clipping method of Denner and Schenke⁶⁰ can treat multivalued solutions at run time, but does not conserve mass and tends to overestimate the attenuation at shock fronts. To remedy this shortcoming, a run-time shock treatment based on a simple averaging procedure of the multivalued solution is proposed, as illustrated in Figure 6. With the overtaking information parcel $i+1$ tagged to be deleted, the location r_i and invariant g_i of information parcel i are redefined as

$$r_{i,j} = \frac{r_{i+1,j} + r_{i,j}}{2} \quad (105)$$

$$g_i = \frac{g_{i+1} + g_i}{2}. \quad (106)$$

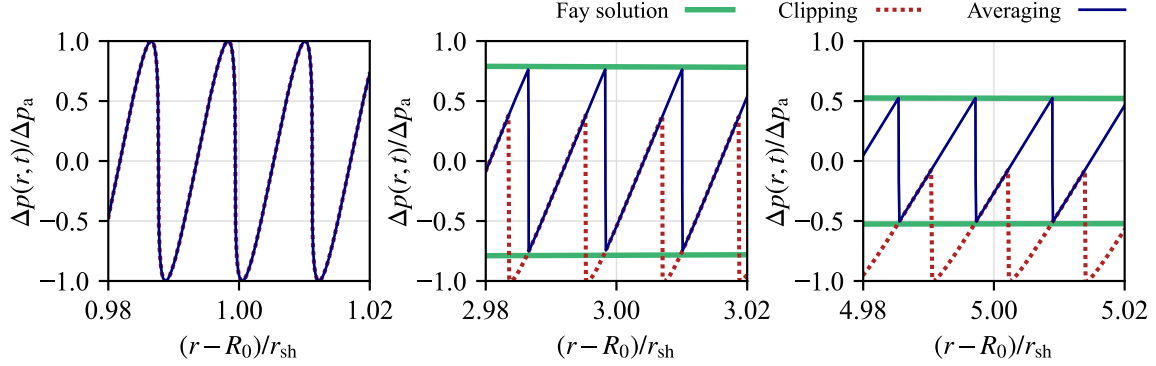


FIG. 7: Pressure amplitude $\Delta p(r, t)$, normalized by the excitation pressure amplitude Δp_a , generated by an oscillating planar emitter as a function of the dimensionless distance $(r - R_0)/r_{\text{sh}}$, where R_0 is the initial size of the emitter and r_{sh} is the shock formation distance of a plane harmonic wave in an inviscid fluid, Eq. (109). The analytical solution for the amplitude of the decaying shock wave of Fay²¹⁸, Eq. (108), is shown for reference.

The average of the invariant g follows from the conservation of specific kinetic enthalpy and presumes that the applied time step is sufficiently small so that the invariant g varies linearly in the close vicinity of the shock front. This leaves the enthalpy h_i and the velocity u_i undefined. Considering that the velocity has two solutions that satisfy a given g , the robust choice is to average the velocity as

$$u_{i,j} = \frac{u_{i+1,j} + u_{i,j}}{2}. \quad (107)$$

The specific enthalpy h_i is then readily defined by Eq. (102). Furthermore, preliminary tests showed that the choice of quantities that are averaged (i.e., g_i and u_i , h_i and u_i , or ρ_i and u_i) has a negligible impact on the results. After the quantities associated with information parcel i have been redefined, the overtaking information parcel $i + 1$ is discarded.

As a first test case, we consider the shock formation of a planar wave emitted in an inviscid fluid by an oscillating planar emitter ($\alpha = 0$). The oscillating emitter generates an harmonic acoustic wave that gradually steepens to eventually form a shock front, at which point it starts to develop into a sawtooth wave that decays due to the attenuation acting at the shock front. For such a sawtooth wave, Fay²¹⁸ derived an analytical solution for the pressure amplitude Δp , given in function of the one-dimensional coordinate r as

$$\Delta p(r) = \pm \frac{\pi r_{\text{sh}}}{r + r_{\text{sh}}} \Delta p_a, \quad (108)$$

where the shock forming distance of a plane harmonic wave is²²⁵

$$r_{\text{sh}} = \frac{\rho_0 c_0^3}{2\pi\beta f_a \Delta p_a}, \quad (109)$$

where f_a and Δp_a are the initial frequency and pressure amplitude of the emitted acoustic wave. The nonlinearity coefficient β for an ideal gas or a Tait fluid is

defined as^{219,226} $\beta = (\gamma + 1)/2$. Note that the solution of Fay, Eq. (108), is only applicable to “perfect” sawtooth waves²²⁵ for $r \gg r_{\text{sh}}$ and that the excitation amplitude Δp_a ought to be sufficiently small such that the nonlinear dependency of the fluid properties on the pressure (see Section IV) is negligible. Figure 7 shows the results obtained using Eqs. (100)-(102) in conjunction with the clipping-based shock treatment of Denner and Schenke⁶⁰ and the averaging-based shock treatment proposed above, for an initially harmonic wave in water modeled using the modified Tait EoS ($\beta = 4.075$). At $r = r_{\text{sh}} + R_0$, the wave profile forms vertical fronts, where $\partial p/\partial r \rightarrow \infty$, as predicted by the theory of Blackstock²²⁵. Subsequently, the wave evolves into a fully developed sawtooth wave and starts to decay, with its amplitude asymptotically approaching the solution of Fay²¹⁸. The clipping procedure of Denner and Schenke⁶⁰, whereby a multivalued solution is treated by clipping the “overtaking” part of the wave profile, fails to predict this sawtooth wave correctly; only the wave peaks reduce, whereas the wave troughs remain unchanged. This shortcoming is evidently less of an issue for the pressure pulses emitted by a strong bubble collapse for which the clipping procedure has previously been tested⁶⁰. The proposed averaging procedure is able to predict the decay of both the peaks and troughs of the sawtooth wave accurately.

To assess the capabilities of the run-time shock treatment in a more representative scenario, the Rayleigh collapse of a spherical gas bubble ($\alpha = 2$) in water is simulated. The bubble has an initial radius R_0 and its collapse is driven by an initial gas pressure of $p_{G,0} = p_\infty/1000$ compared to a constant ambient pressure of $p_\infty = 10^5$ Pa. The gas is modeled using the NA EoS, see Eqs. (59) and (60), with $\rho_{G,0} = 1.2 \text{ kg/m}^3$ at p_∞ , $\kappa = 1.4$, and $b = 1.5 \times 10^{-3} \text{ m}^3/\text{kg}$, whereas water is modeled using the modified Tait EoS, with $n = 7.15$, $B = 3.046 \times 10^8 \text{ Pa}$, $\rho_0 = 997 \text{ kg/m}^3$ at p_∞ , and $\mu = 0.001 \text{ Pa s}$. The surface tension of the gas-liquid interface is neglected. For validation purposes, the results obtained based on the

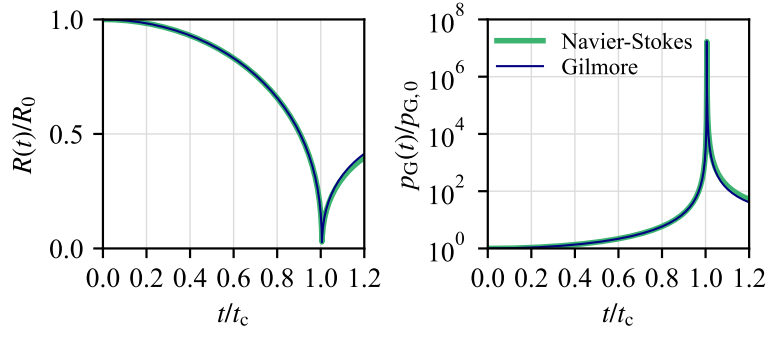


FIG. 8: Radius $R(t)$, normalized by the initial radius R_0 , and gas pressure $p_G(t)$, normalized by the initial gas pressure $p_{G,0}$, as a function of time t , normalized by the Rayleigh collapse time t_c , of the Rayleigh collapse of a spherical gas bubble in water, obtained with a Navier-Stokes solver and the Gilmore equation.

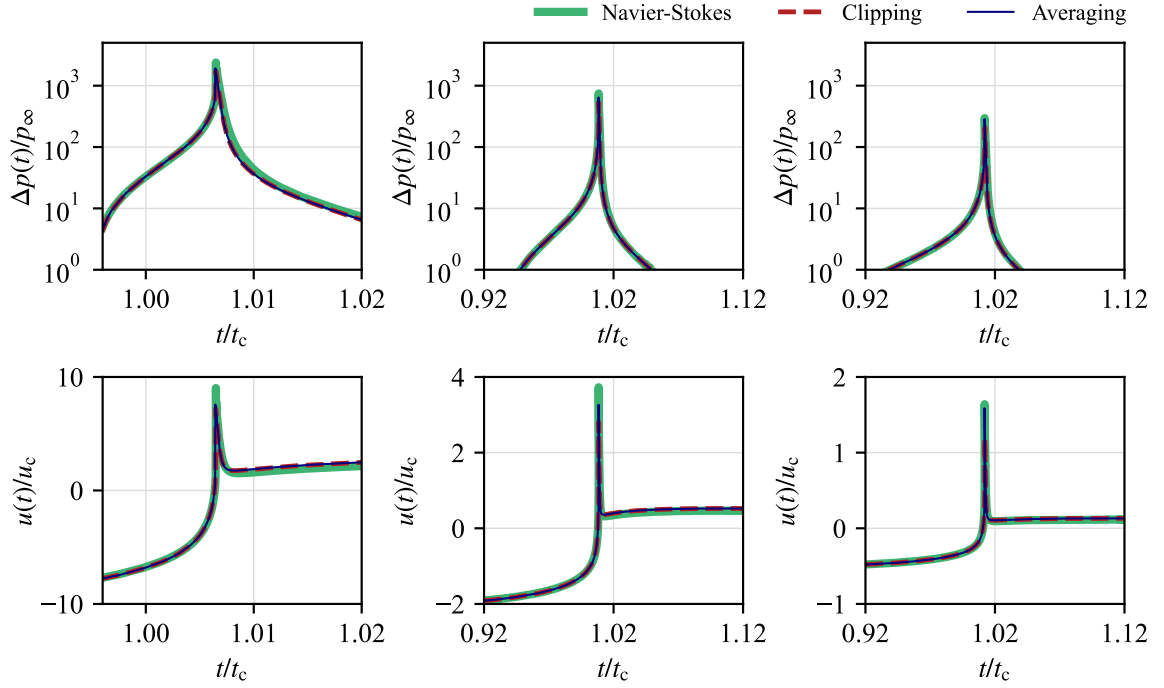


FIG. 9: Temporal evolution of the pressure amplitude $\Delta p(r, t) = p(r, t) - p_\infty$, normalized by the constant ambient pressure p_∞ , and flow velocity $u(r, t)$, normalized by the characteristic collapse velocity $u_c = R_0/t_c$, emitted by the Rayleigh collapse of a spherical gas bubble in water at different radial locations $r = \{0.2, 0.5, 1\}R_0$, obtained with the KBH model described in Section VIII B. Time t is normalized by the Rayleigh collapse time t_c . The multivalued solutions at the shock front are treated either by clipping the wave profile or by applying the proposed averaging procedure. Results obtained with a Navier-Stokes solver are shown for reference.

Kirkwood-Bethe hypothesis are compared to a fully resolved simulation using a state-of-the-art Navier-Stokes solver^{46,52}. For this simulation, the pressure in the liquid is initialized as $p(r) = p_\infty + R_0(p_{G,0} - p_\infty)/r$, the bubble is resolved with 1000 mesh cells per initial bubble radius, and the time step applied at the time when the bubble reaches its minimum radius is $\Delta t \simeq 5 \times 10^{-8}t_c$, where $t_c \simeq 0.915 R_0 \sqrt{\rho_\infty/p_\infty}$ is the Rayleigh collapse time²²⁷. Figure 8 shows a close agreement of the bubble radius and gas pressure obtained with the Navier-Stokes solver and

with the Gilmore equation, Eq. (55). The temporal evolution of the pressure and velocity in the vicinity of the bubble is shown in Figure 9, at $r = \{0.2, 0.5, 1\}R_0$. The emitted acoustic wave forms a shock front, with a vertical left slope of the pressure and velocity profiles. Note that in the temporal-evolution plots shown in Figure 9, the left-hand side of the profile reaches the measurement location first. The results obtained with both methods to treat the shock front, either clipping the wave profile or applying the proposed averaging procedure, yield a good

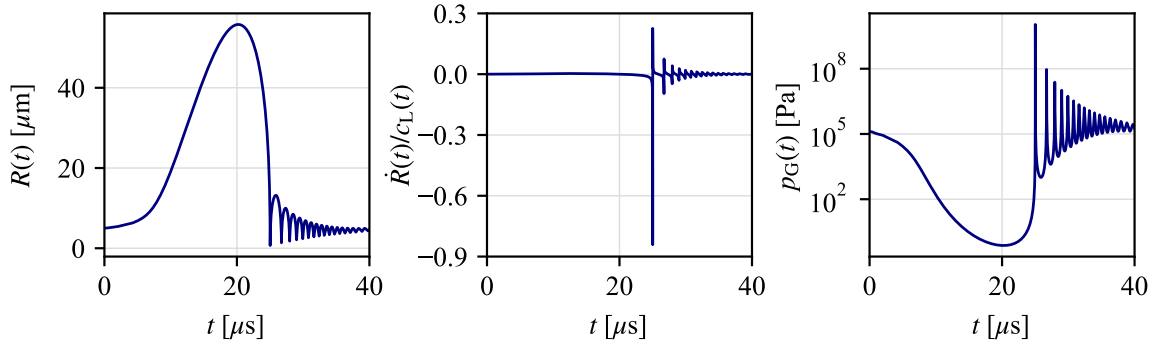


FIG. 10: Temporal evolution of the radius $R(t)$, bubble wall Mach number $\dot{R}(t)/c_L(t)$, and gas pressure $p_G(t)$ of the sonoluminescence bubble of Holzfluss¹⁶³, obtained with the Gilmore model.

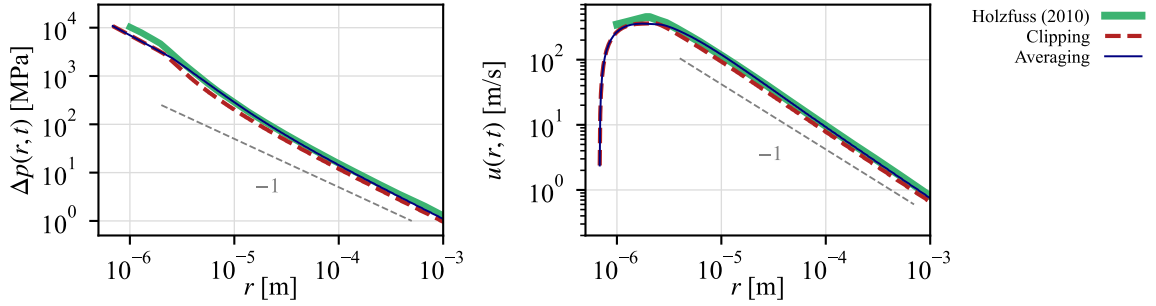


FIG. 11: Spatial evolution of the pressure amplitude $\Delta p(r, t) = p(r, t) - p_\infty(t)$ and the flow velocity $u(r, t)$ of the acoustic wave emitted by the primary collapse of the sonoluminescence bubble of Holzfluss¹⁶³, obtained with the KBH model described in Section VIII B. The multivalued solutions at the shock front are treated either by clipping the wave profile or by applying the proposed averaging procedure. The expected pressure and velocity decay in the far field, proportional to r^{-1} , is indicated by the gray dashed lines.

agreement with the Navier-Stokes solution for this specific test case. However, clipping the wave profile overpredicts the attenuation of the shock front in the far field, which manifests in a smaller peak pressure and velocity at $r = R_0$.

The strong collapse and shock formation of an argon bubble that produces sonoluminescence¹⁶³ and of a laser-induced bubble⁵⁹ have previously been studied with respect to the emission of shock waves using KBH models. In both studies^{59,163}, the rule of equal areas was applied to rectify the multivalued solutions at the shock front. The sonoluminescence bubble considered by Holzfluss¹⁶³ has an initial radius of $R_0 = 5 \mu\text{m}$ and is excited with a frequency of $f_a = 23.5 \text{ kHz}$ and a pressure amplitude of $\Delta p_a = 145 \text{ kPa}$, whereas the laser-induced bubble studied by Liang *et al.*⁵⁹ is generated by a laser pulse with $20 \mu\text{J}$ energy and 265 fs duration, and reaches a maximum bubble radius of approximately $36 \mu\text{m}$. In both cases, water is modeled by the modified Tait EoS. The exact parameters of these cases can be found in the respective publications, or the recent work of Denner and Schenke⁶⁰. For orientation, the radius R , bubble wall Mach number \dot{R}/c_L , and gas pressure p_G of the sonoluminescence and laser-induced bubbles are shown as a function of time

in Figures 10 and 12, respectively. Note that the discontinuous changes in gas pressure of the laser-induced bubble are intentional and account for the complex mass-transfer dynamics of this bubble, as proposed by Liang *et al.*⁵⁹. In Figure 11, the pressure and velocity amplitude of the acoustic wave emitted by the primary collapse of the sonoluminescence bubble are shown, where subtle differences can be observed dependent on the treatment of the developing shock front. The proposed averaging procedure exhibits a tendency to larger pressure and velocity values compared to simply clipping the wave profile. Nevertheless, the results obtained with both methods to treat the shock front at run time compare very well with the results of Holzfluss¹⁶³. The spatial profiles of the acoustic wave produced by the collapse of the laser-induced bubble, see Figure 13, exhibit a comparable trend: the proposed averaging procedure yields a faster shock front with larger pressure and velocity values compared to both the results of Liang *et al.*⁵⁹ and the results obtained by clipping the wave profile. The observed differences are confined to the immediate vicinity of the shock front and are largest in the region in which the shock dissipation is strongest.

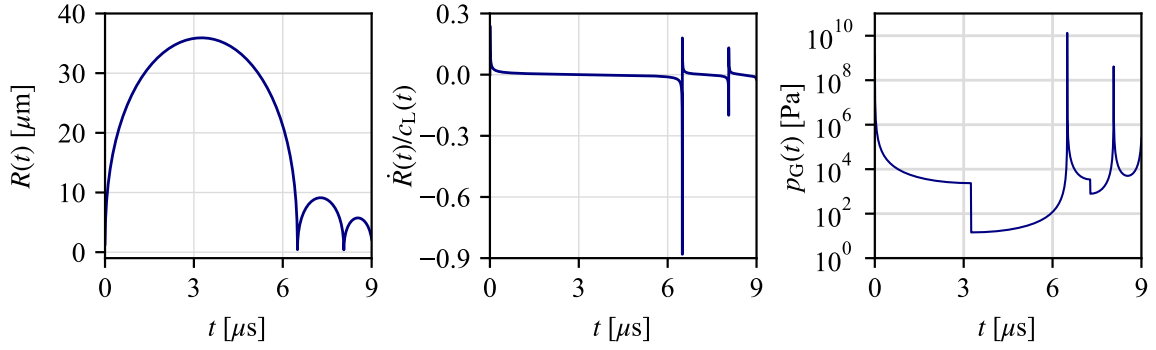


FIG. 12: Temporal evolution of the radius $R(t)$, bubble wall Mach number $\dot{R}(t)/c_L(t)$, and gas pressure $p_G(t)$ of the laser-induced bubble of Liang *et al.*⁵⁹, obtained with the Gilmore model.

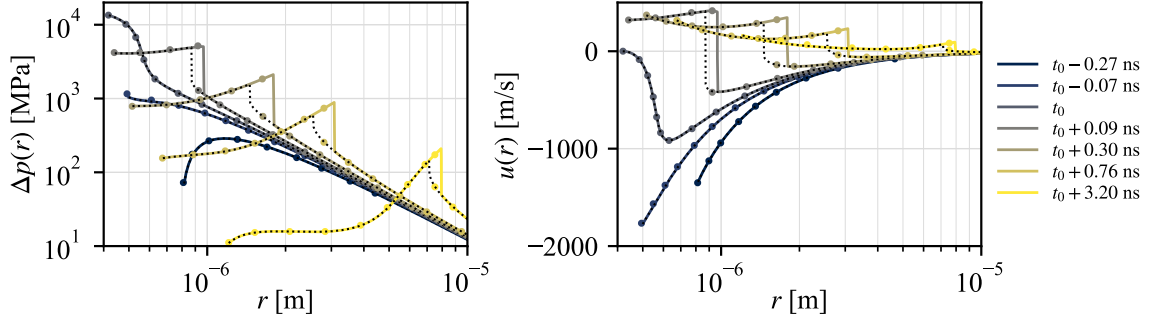


FIG. 13: Wave profiles of the pressure amplitude $\Delta p(r, t) = p(r, t) - p_\infty(t)$ and the flow velocity $u(r, t)$ at selected time instances of the acoustic wave emitted by the first collapse of the laser-induced bubble of Liang *et al.*⁵⁹, obtained with the KBH model described in Section VIII B. The solid line shows the results obtained by applying the proposed averaging procedure at the shock front, the dotted line shows the results obtained by clipping the wave profile, and the colored dots show the corresponding results of Liang *et al.*⁵⁹. Time t_0 is the time at which the peak pressure is emitted.

B. Complex impedance of curved acoustic waves

The acoustic impedance experienced by a curved acoustic wave is complex, see Eq. (37), and depends on the radius of curvature of the acoustic wave relative to its wavenumber. Only for relatively short waves ($kr \gg 1$) does the simple definition $z = \rho c$ of the specific acoustic impedance hold in good approximation.

As discussed in Section VI A, the explicit velocity expression given by Eq. (69) is the sum of the displacement of the fluid by the moving gas-liquid interface and the acoustic particle velocity associated with the emitted acoustic wave. According to Eq. (69), the acoustic particle velocity u_1 is, thus, given as

$$u_1(r, t) = \left[\frac{R(\tau)}{r(t)} \right]^{\alpha/2} \frac{h_L(\tau) - h_\infty(\tau)}{c(r, t) + u(r, t)}. \quad (110)$$

Applying the isentropic relation $dh = dp/\rho$ and assuming the acoustic wave has a small pressure amplitude, such that $u \ll c$, $\rho = \rho(r, t) = \rho_L(\tau)$ and $c = c(r, t) = c_L(\tau)$,

the velocity is

$$u_1(r, t) = \left[\frac{R(\tau)}{r(t)} \right]^{\alpha/2} \frac{p_L(\tau) - p_\infty(\tau)}{\rho c}, \quad (111)$$

or, using the notation used in the acoustic expansions, with $p = p_0 + p_1$,

$$u_1(r, t) = \left[\frac{R(\tau)}{r(t)} \right]^{\alpha/2} \frac{p_1(\tau)}{\rho c}. \quad (112)$$

This expression is evidently not dependent on the relative curvature of the emitted wave and, therefore, suggests that velocity expressions derived from the Kirkwood-Bethe hypothesis do not account for the complex acoustic impedance of curved waves.

To test this, we consider a spherical emitter situated in water that oscillates and emits acoustic waves at angular frequency ω_a , chosen such that a specific dimensionless wavenumber $k_a R_0$ is obtained, with $k_a = \omega_a/c$. The pressure at the emitter wall and the time-dependent velocity

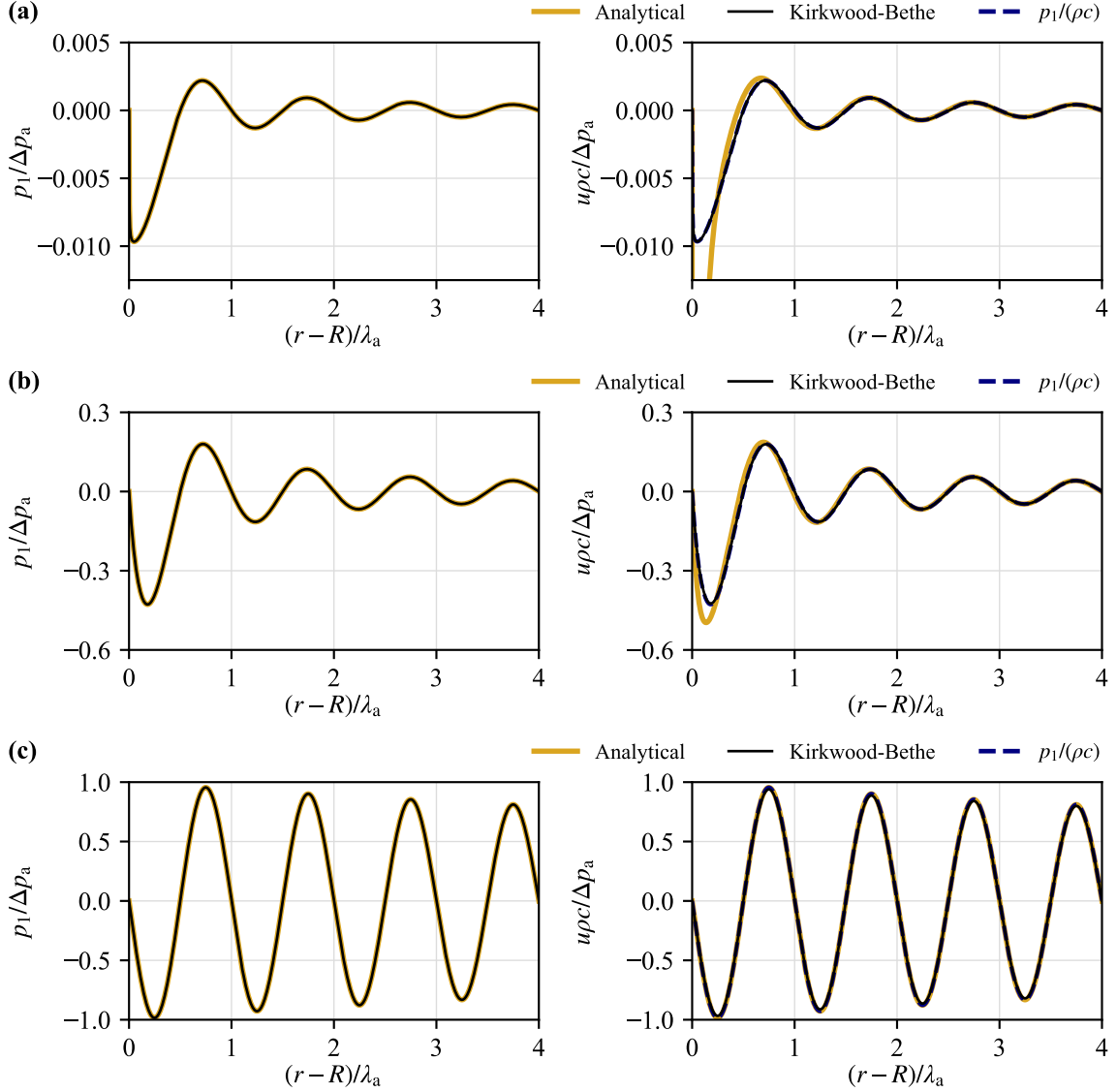


FIG. 14: The pressure (left) and velocity (right) of acoustic waves emitted by a pulsating spherical emitter with (a) $k_a R_0 = 0.01$, (b) $k_a R_0 = 1$, and (c) $k_a R_0 = 100$, predicted by the Kirkwood-Bethe hypothesis. The analytical solution for curved acoustic waves, Eqs. (115) and (117), and the particle velocity for plane acoustic waves are shown for reference.

of the emitter wall are defined as

$$p_L(t) = p_0 + \Delta p_a \cos\left(\omega_a t - \frac{\pi}{2}\right) \quad (113)$$

$$\dot{R}(t) = \frac{\Delta p_a}{\rho c} \cos\left(\omega_a t - \frac{\pi}{2}\right), \quad (114)$$

respectively. The considered pressure amplitude Δp_a is sufficiently small such that the pressure-dependency of the liquid density and speed of sound are negligible. At the emitter wall, pressure and velocity are, therefore, in phase and there is no relative velocity between the emitter wall and the fluid. The water surrounding the emitter is described using the modified Tait EoS, with $n = 7.15$, $B = 3.046 \times 10^8$ Pa, and $\rho_0 = 997$ kg/m³. Following

Eq. (37), the analytical solutions for the acoustic pressure and particle velocity are given as¹⁸²

$$p_1(r, t) = \frac{R}{r} \Delta p_a \cos\left(\omega_a t - \frac{\pi}{2} - k(r - R)\right) \quad (115)$$

$$u_1(r, t) = \frac{R}{r} \frac{\Delta p_a}{\rho c \cos(\theta)} \cos\left(\omega_a t - \frac{\pi}{2} - k(r - R) - \theta\right), \quad (116)$$

respectively, where the complex impedance manifests in the phase shift $\theta = \pi/2 - \arctan(kr)$. Taking the oscillating emitter into account by inserting the analytical particle velocity defined by Eq. (116) into the flow velocity given by Eq. (67), the analytical solution for the flow

velocity is

$$u(r, t) = \frac{R^2}{r^2} \dot{R}(t) - \frac{R}{r} u_1(r, t) + u_1(r, t). \quad (117)$$

Figure 14 shows the spatial profiles of the pressure and velocity generated by the spherical emitter ($\alpha = 2$) for $k_a R_0 \in \{0.01, 1, 100\}$, predicted by the Kirkwood-Bethe hypothesis, using Eqs. (100)-(102). For all three cases, the pressure predicted by the Kirkwood-Bethe hypothesis is in virtually perfect agreement with the analytical solution, Eq. (115). However, the velocity profile predicted by the Kirkwood-Bethe hypothesis agrees with the analytical solution for a curved wave, Eq. (117), only for the case with $k_a R_0 = 10^2$, i.e. for a short wave with $kr \gg 1$. As the dimensionless wavenumber decreases, i.e. longer waves, the accuracy of the velocity predicted by the Kirkwood-Bethe hypothesis deteriorates near the emitter. Despite this shortcoming, the Kirkwood-Bethe hypothesis predicts the velocity accurately after the wave has traveled for more than approximately one wavelength λ_a , which corresponds to $k_a(r - R_0) \gtrsim 2\pi$. We can, therefore, conclude that the Kirkwood-Bethe hypothesis does not account for the complex acoustic impedance of curved waves and, as a consequence, fails to predict the particle velocity of long waves ($kr \lesssim 1$) close to the emitter correctly. In fact, the velocity ODE arising from the Kirkwood-Bethe hypothesis, Eq. (101), predicts $u_1 \simeq p_1/(\rho c)$ for all three cases, as observed in Figure 14, irrespective of the dimensionless wavenumber kr . Nevertheless, the predictions provided by the Kirkwood-Bethe hypothesis are accurate for $r \gtrsim R + \lambda_a$.

Recent experimental and numerical studies that reported accurate predictions of KBH models stand in apparent contradiction to the shortcoming associated with the complex nature of the acoustic impedance. For instance, the experimental measurements of the pressure and velocity of shock waves emitted by laser-induced cavitation bubbles of Lai *et al.*⁵⁸ and the fully resolved numerical results of the Rayleigh collapse of a spherical gas bubble shown in Figure 9 are in very good agreement with the corresponding predictions provided on the basis of the Kirkwood-Bethe hypothesis. However, in these cases, which are representative for pressure-driven bubble dynamics, including underwater explosions as well as medical and sonochemical applications, the length of the emitted pressure pulse is short, with $kR = \mathcal{O}(1)$ or larger⁵⁸⁻⁶¹. In addition, the velocity very close to the bubble is dominated by the motion of the gas-liquid interface and even though the particle velocity is nominally large, it is typically less than 10% of the total propagation velocity $c + u$.

X. CONCLUSIONS

Originally developed to estimate the peak pressure of an underwater explosion at some distance, the Kirkwood-Bethe hypothesis has given rise to a collection of models

that describe pressure-driven bubble dynamics, cavitation and underwater explosions, as well as their acoustic emissions, with remarkable accuracy. By using standard numerical integration methods and modern computational equipment, these models allow to predict complex processes of fluid dynamics and nonlinear acoustics, such as the laser-induced cavitation bubble discussed in Section IX A, in a fraction of a second. Here, the theoretical foundations of the Kirkwood-Bethe hypothesis and contemporary models derived from it have been reviewed, as well as generalized from the typically considered spherical symmetry, to account for spherically symmetric, cylindrically symmetric, and planar one-dimensional domains. In addition, a new method to treat multivalued solutions associated with the formation of shock fronts at simulation run time has been proposed, which further improves the predictive capabilities of the models based on the Kirkwood-Bethe hypothesis. Even though the Kirkwood-Bethe hypothesis fails to account for the curvature of acoustic waves, as they are, for instance, emitted by a bubble collapse, it has been shown to provide accurate predictions under the specific conditions associated with pressure-driven bubble dynamics, cavitation and underwater explosions.

Despite the extensive and formidable work achieved by the research community over more than eight decades, models based on the Kirkwood-Bethe hypothesis still lack some basic capabilities that can further extend their applicability and improve their accuracy. For instance, although the Kirkwood-Bethe hypothesis can produce accurate pressure and velocity predictions under realistic scenarios, it does not account for heat transfer. As a first step, the recent combination of the Kirkwood-Bethe hypothesis with the Noble-Abel stiffened-gas equation of state for bubble dynamics⁹⁰ and acoustic emissions⁶⁰ provides a consistent and accurate basis for predicting the temperature in the liquid surrounding a gas bubble or cavity. While adiabatic temperature changes can be readily predicted in this way, thermal conduction and viscous heating, such as the heat introduced by the energy dissipation at a shock front⁵⁹, are not accounted for. In this respect, medical ultrasound stands out as a field that requires high-fidelity temperature predictions if computational tools are to play a more prominent role in the design of new treatments, since temperature changes of only 1 K can be safety relevant²²⁸. More generally, bubbles are neither stationary nor do they appear in isolation or in a liquid of quasi-infinite extent in most engineering applications, which contradicts some of the main assumptions underpinning the available models based on the Kirkwood-Bethe hypothesis. Recent advances for methods developed based on the (quasi-)acoustic assumption point to possible solutions that may be incorporated into models based on the Kirkwood-Bethe hypothesis, to account for the forces on bubbles as they move through a liquid¹⁸⁶, the acoustic interaction of multiple bubbles²²⁹, and the influence of confinement and nearby walls²³⁰.

CONFLICT OF INTEREST

The author has no conflicts that could have influenced this work.

DATA AVAILABILITY

All presented results were produced, and can be readily reproduced, with the open-source software library APECSS, as referenced in Section IX.

REFERENCES

- 1 M. S. Plesset and A. Prosperetti, "Bubble Dynamics and Cavitation," *Annual Review of Fluid Mechanics* **9**, 145–185 (1977).
- 2 C. E. Brennen, *Cavitation and Bubble Dynamics*, Oxford Engineering Science Series No. 44 (Oxford University Press, New York, 1995).
- 3 W. Lauterborn and T. Kurz, "Physics of bubble oscillations," *Reports on Progress in Physics* **73**, 106501 (2010).
- 4 J. R. Blake and D. C. Gibson, "Cavitation Bubbles Near Boundaries," *Annual Review of Fluid Mechanics* **19**, 99–123 (1987).
- 5 F. Reuter, C. Deiter, and C.-D. Ohl, "Cavitation erosion by shockwave self-focusing of a single bubble," *Ultrasonics Sonochemistry* **90**, 106131 (2022).
- 6 M. Dular and C. D. Ohl, "Bulk material influence on the aggressiveness of cavitation – Questioning the microjet impact influence and suggesting a possible way to erosion mitigation," *Wear* , 205061 (2023).
- 7 K. Johansen, J. H. Song, K. Johnston, and P. Prentice, "Deconvolution of acoustically detected bubble-collapse shock waves," *Ultrasonics* **73**, 144–153 (2017).
- 8 L. Gaisser, O. Kirschner, and S. Riedelbauch, "Cavitation detection in hydraulic machinery by analyzing acoustic emissions under strong domain shifts using neural networks," *Physics of Fluids* **35**, 027128 (2023).
- 9 S. C. Haskell, N. Lu, G. E. Stocker, Z. Xu, and J. R. Sukovich, "Monitoring cavitation dynamics evolution in tissue mimicking hydrogels for repeated exposures via acoustic cavitation emissions," *The Journal of the Acoustical Society of America* **153**, 237–247 (2023).
- 10 M. Wan, Y. Feng, and G. ter Haar, eds., *Cavitation in Biomedicine* (Springer Netherlands, Dordrecht, 2015).
- 11 D. Meroni, R. Djellabi, M. Ashokkumar, C. L. Bianchi, and D. C. Boffito, "Sonoprocessing: From Concepts to Large-Scale Reactors," *Chemical Reviews* **122**, 3219–3258 (2022).
- 12 K. Maeda, A. D. Maxwell, T. Colonius, W. Kreider, and M. R. Bailey, "Energy shielding by cavitation bubble clouds in burst wave lithotripsy," *The Journal of the Acoustical Society of America* **144**, 2952–2961 (2018).
- 13 O. A. Sapozhnikov, A. D. Maxwell, and M. R. Bailey, "Maximizing mechanical stress in small urinary stones during burst wave lithotripsy," *The Journal of the Acoustical Society of America* **150**, 4203–4212 (2021).
- 14 E. Yeats, N. Lu, J. R. Sukovich, Z. Xu, and T. L. Hall, "Soft Tissue Aberration Correction for Histotripsy Using Acoustic Emissions From Cavitation Cloud Nucleation and Collapse," *Ultrasound in Medicine & Biology* **49**, 1182–1193 (2023).
- 15 A. Vogel, W. Hentschel, J. Holzfuss, and W. Lauterborn, "Cavitation Bubble Dynamics and Acoustic Transient Generation in Ocular Surgery with Pulsed Neodymium:YAG Lasers," *Ophthalmology* **93**, 1259–1269 (1986).
- 16 T. Lee, W. Luo, Q. Li, H. Demirci, and L. J. Guo, "Laser-Induced Focused Ultrasound for Cavitation Treatment: Toward High-Precision Invisible Sonic Scalpel," *Small* **13**, 1701555 (2017).
- 17 G. Shakya, M. Cattaneo, G. Guerriero, A. Prasanna, S. Fiorini, and O. Supponen, "Ultrasound-responsive microbubbles and nanodroplets: A pathway to targeted drug delivery," *Advanced Drug Delivery Reviews* **206**, 115178 (2024).
- 18 M. Habibi, S. Foroughi, V. Karamzadeh, and M. Packirisamy, "Direct sound printing," *Nature Communications* **13**, 1800 (2022).
- 19 A. G. Athanassiadis, Z. Ma, N. Moreno-Gomez, K. Melde, E. Choi, R. Goyal, and P. Fischer, "Ultrasound-Responsive Systems as Components for Smart Materials," *Chemical Reviews* **122**, 5165–5208 (2022).
- 20 Z. Ma, C. Bourquard, Q. Gao, S. Jiang, T. De Iure-Grimmel, R. Huo, X. Li, Z. He, Z. Yang, G. Yang, Y. Wang, E. Lam, Z.-h. Gao, O. Supponen, and J. Li, "Controlled tough bioadhesion mediated by ultrasound," *Science* **377**, 751–755 (2022).
- 21 C.-D. Ohl, M. Arora, R. Ikink, N. de Jong, M. Versluis, M. Delius, and D. Lohse, "Sonoporation from Jetting Cavitation Bubbles," *Biophysical Journal* **91**, 4285–4295 (2006).
- 22 B. Helfield, X. Chen, S. C. Watkins, and F. S. Villanueva, "Biophysical insight into mechanisms of sonoporation," *Proceedings of the National Academy of Sciences* **113**, 9983–9988 (2016).
- 23 A. Šarc, J. Kosel, D. Stopar, M. Oder, and M. Dular, "Removal of bacteria *Legionella pneumophila*, *Escherichia coli*, and *Bacillus subtilis* by (super)cavitation," *Ultrasonics Sonochemistry* **42**, 228–236 (2018).
- 24 G. L. Chahine, A. Kapahi, J.-K. Choi, and C.-T. Hsiao, "Modeling of surface cleaning by cavitation bubble dynamics and collapse," *Ultrasonics Sonochemistry* **29**, 528–549 (2016).
- 25 F. Reuter, S. Lauterborn, R. Mettin, and W. Lauterborn, "Membrane cleaning with ultrasonically driven bubbles," *Ultrasonics Sonochemistry* **37**, 542–560 (2017).
- 26 S. Barcikowski, A. Plech, K. S. Suslick, and A. Vogel, "Materials synthesis in a bubble," *MRS Bulletin* **44**, 382–391 (2019).
- 27 H. Soyama and A. M. Korsunsky, "A critical comparative review of cavitation peening and other surface peening methods," *Journal of Materials Processing Technology* **305**, 117586 (2022).
- 28 U. J. Gutiérrez-Hernández, H. Reese, F. Reuter, C.-D. Ohl, and P. A. Quinto-Su, "Nano-Cracks and Glass Carving from Non-Symmetrically Converging Shocks," *Advanced Physics Research* , 2300030 (2023).
- 29 C. Llorens, M. Argentina, N. Rojas, J. Westbrook, J. Dumais, and X. Noblin, "The fern cavitation catapult: Mechanism and design principles," *Journal of The Royal Society Interface* **13**, 20150930 (2016).
- 30 P. Koukouviniis, C. Bruecker, and M. Gavaises, "Unveiling the physical mechanism behind pistol shrimp cavitation," *Scientific Reports* **7**, 13994 (2017).
- 31 R. H. Cole, *Underwater Explosions* (Princeton University Press, Princeton, New Jersey, 1948).
- 32 W. Wu, A.-M. Zhang, Y.-L. Liu, and M. Liu, "Interaction between shock wave and a movable sphere with cavitation effects in shallow water," *Physics of Fluids* **32**, 016103 (2020).
- 33 W. Yu, S. Song, and J.-I. Choi, "Numerical simulations of underwater explosions using a compressible multi-fluid model," *Physics of Fluids* **35**, 106102 (2023).
- 34 K. de Graaf, I. Penesis, and P. Brandner, "Modelling of seismic airgun bubble dynamics and pressure field using the Gilmore equation with additional damping factors," *Ocean Engineering* **76**, 32–39 (2014).
- 35 A. O. MacGillivray, "An Airgun Array Source Model Accounting for High-Frequency Sound Emissions During Firing—Solutions to the IAMW Source Test Cases," *IEEE Journal of Oceanic Engineering* **44**, 582–588 (2019).
- 36 A. G. Athanassiadis, *Optical Breakdown Acoustics: Transduction and Sensing Underwater*, Ph.D. thesis, Massachusetts Institute of Technology, Cambridge, MA, USA (2019).
- 37 M. A. O'Reilly and K. Hynnenen, "Blood-Brain Barrier: Real-time Feedback-controlled Focused Ultrasound Disruption by Us-

- ing an Acoustic Emissions-based Controller,” *Radiology* **263**, 96–106 (2012).
- ³⁸A. Novell, H. A. S. Kamimura, A. Cafarelli, M. Gerstenmayer, J. Flament, J. Valette, P. Agou, A. Conti, E. Selingue, R. Aron Badin, P. Hantraye, and B. Larrat, “A new safety index based on intrapulse monitoring of ultra-harmonic cavitation during ultrasound-induced blood-brain barrier opening procedures,” *Scientific Reports* **10**, 10088 (2020).
- ³⁹V.-S. Doan, T. Huynh-The, and D.-S. Kim, “Underwater Acoustic Target Classification Based on Dense Convolutional Neural Network,” *IEEE Geoscience and Remote Sensing Letters* **19**, 1500905 (2022).
- ⁴⁰M. Rom, “Physics-informed neural networks for the Reynolds equation with cavitation modeling,” *Tribology International* **179**, 108141 (2023).
- ⁴¹K. Klapcsik, B. Gyires-Tóth, J. M. Rosselló, and F. Hegedűs, “Position control of an acoustic cavitation bubble by reinforcement learning,” (2023), [arxiv:2312.05674 \[cs, eess\]](https://arxiv.org/abs/2312.05674).
- ⁴²W. Mallik, R. Jaiman, and J. Jelovica, “Deep neural network for learning wave scattering and interference of underwater acoustics,” *Physics of Fluids* **36**, 017137 (2024).
- ⁴³J. G. Kirkwood and H. A. Bethe, “The pressure wave produced by an underwater explosion I,” Tech. Rep. Report No. 588 (Office of Scientific Research and Development, 1942).
- ⁴⁴R. Ivany, *Collapse of a Cavitation Bubble in Viscous Compressible Liquid: Numerical and Experimental Analysis*, Ph.D. thesis, University of Michigan, Ann Arbor, MI, USA (1965).
- ⁴⁵R. R. Lilliston, “Calculations on the collapse of a spherical gas-filled cavity in a compressible liquid,” Tech. Rep. 2223 (SP 6-0002) (David Taylor Model Basin, Washington, DC, USA, 1966).
- ⁴⁶F. Denner, C.-N. Xiao, and B. van Wachem, “Pressure-based algorithm for compressible interfacial flows with acoustically-conservative interface discretisation,” *Journal of Computational Physics* **367**, 192–234 (2018).
- ⁴⁷D. Fuster and S. Popinet, “An all-Mach method for the simulation of bubble dynamics problems in the presence of surface tension,” *Journal of Computational Physics* **374**, 752–768 (2018).
- ⁴⁸K. Schmidmayer, F. Petitpas, S. Le Martelot, and É. Daniel, “ECOGEN: An open-source tool for multiphase, compressible, multiphysics flows,” *Computer Physics Communications* **251**, 107093 (2020).
- ⁴⁹S. H. Bryngelson, K. Schmidmayer, V. Coralic, J. C. Meng, K. Maeda, and T. Colonius, “MFC: An open-source high-order multi-component, multi-phase, and multi-scale compressible flow solver,” *Computer Physics Communications* **266**, 107396 (2021).
- ⁵⁰Y. Saade, D. Lohse, and D. Fuster, “A multigrid solver for the coupled pressure-temperature equations in an all-Mach solver with VoF,” *Journal of Computational Physics* **476**, 111865 (2023).
- ⁵¹M. Koch, C. Lechner, F. Reuter, K. Köhler, R. Mettin, and W. Lauterborn, “Numerical modeling of laser generated cavitation bubbles with the finite volume and volume of fluid method, using OpenFOAM,” *Computers & Fluids* **126**, 71–90 (2016).
- ⁵²F. Denner, F. Evrard, and B. van Wachem, “Modeling Acoustic Cavitation Using a Pressure-Based Algorithm for Polyotropic Fluids,” *Fluids* **5**, 69 (2020).
- ⁵³S. R. Gonzalez-Avila, F. Denner, and C.-D. Ohl, “The acoustic pressure generated by the cavitation bubble expansion and collapse near a rigid wall,” *Physics of Fluids* **33**, 032118 (2021).
- ⁵⁴S.-P. Wang, H. Geng, S. Zhang, and S.-W. Wang, “Pressure waves from air gun bubbles: A numerical analysis based on the finite volume method,” *Physics of Fluids* **36**, 013345 (2024).
- ⁵⁵D. G. Crighton, A. P. Dowling, J. E. Ffowcs Williams, M. Heckl, and F. G. Leppington, *Modern Methods in Analytical Acoustics* (Springer London, London, 1992).
- ⁵⁶I. C. Christov and C. I. Christov, “On mechanical waves and Doppler shifts from moving boundaries,” *Mathematical Methods in the Applied Sciences* **40**, 4481–4492 (2017).
- ⁵⁷F. Denner, “Acoustic pressure modulation driven by spatially non-uniform flow,” *Journal of the Acoustical Society of America* **155**, 984–989 (2024).
- ⁵⁸G. Lai, S. Geng, H. Zheng, Z. Yao, Q. Zhong, and F. Wang, “Early Dynamics of a Laser-Induced Underwater Shock Wave,” *Journal of Fluids Engineering* **144**, 011501 (2022).
- ⁵⁹X.-X. Liang, N. Linz, S. Freidank, G. Paltauf, and A. Vogel, “Comprehensive analysis of spherical bubble oscillations and shock wave emission in laser-induced cavitation,” *Journal of Fluid Mechanics* **940**, A5 (2022).
- ⁶⁰F. Denner and S. Schenke, “Modeling acoustic emissions and shock formation of cavitation bubbles,” *Physics of Fluids* **35**, 012114 (2023).
- ⁶¹H. Wen, Z. Yao, Q. Zhong, Y. Tian, Y. Sun, and F. Wang, “Energy partitioning in laser-induced millimeter-sized spherical cavitation up to the fourth oscillation,” *Ultrasonics Sonochemistry* **95**, 106391 (2023).
- ⁶²F. R. Gilmore, “The growth or collapse of a spherical bubble in a viscous compressible liquid,” Tech. Rep. Report No. 26-4 (California Institute of Technology, Pasadena, California, USA, 1952).
- ⁶³H. G. Flynn, “Collapse of a transient cavity in a compressible liquid,” Technical Memorandum 38 (Acoustics Research Laboratory, Harvard University, Cambridge, MA, USA, 1957).
- ⁶⁴R. Hickling and M. S. Plesset, “The collapse of a spherical cavity in a compressible liquid,” Tech. Rep. 85-24 (California Institute of Technology, Pasadena, California, USA, 1963).
- ⁶⁵R. T. Beyer, “Nonlinear Acoustics,” Technical Report (Brown University, Providence, RI, USA, 1974).
- ⁶⁶H. G. Flynn, “Cavitation dynamics: IV. Collapse of transient cavities,” Tech. Rep. (University of Rochester, Rochester, NY, USA, 1978).
- ⁶⁷O. K. Rice and R. Ginell, “The pressure wave produced by an underwater explosion: Part VI: The case of cylindrical symmetry,” Tech. Rep. 2023 (Office of Scientific Research and Development, 1943).
- ⁶⁸O. K. Rice and R. Ginell, “The pressure wave produced by an underwater explosion, Part VIII. The case of cylindrical symmetry, II,” Tech. Rep. 3950 (Office of Scientific Research and Development, 1944).
- ⁶⁹G. B. Whitham, “Spherical waves and shocks,” Tech. Rep. IMM-NYU 190 (Courant Institute of Mathematical Sciences, New York University, New York, NY, USA, 1953).
- ⁷⁰H. Snay, “Hydrodynamic concepts: Selected topics for underwater nuclear explosions,” Technical Report NOLTR 65-52 (US Naval Ordnance Laboratory, White Oak, MD, USA, 1966).
- ⁷¹K. A. Naugol’nykh and N. A. Roy, “Electrical discharges in water: A hydrodynamic description,” Tech. Rep. (Academy of Sciences USSR, Acoustic Institute, Moscow, 1971).
- ⁷²R. Cooper, ed., *Second Symposium on Naval Hydrodynamics: Hydrodynamic Noise, Cavity Flow* (National Academy of Sciences–National Research Council, 1958).
- ⁷³L. D. Rozenberg, ed., *High-Intensity Ultrasonic Fields* (Springer US, Boston, MA, 1971).
- ⁷⁴W. Lauterborn, ed., *Cavitation and Inhomogeneities in Underwater Acoustics* (Springer Berlin Heidelberg, Berlin, Heidelberg, 1980).
- ⁷⁵A. Schneider, *Some Compressibility Effects in Cavitation Bubble Dynamics*, Ph.D. thesis, California Institute of Technology, Pasadena, California, USA (1949).
- ⁷⁶R. Hickling and M. S. Plesset, “Collapse and Rebound of a Spherical Bubble in Water,” *Physics of Fluids* **7**, 7–14 (1964).
- ⁷⁷R. D. Ivany and F. G. Hammitt, “Cavitation Bubble Collapse in Viscous, Compressible Liquids—Numerical Analysis,” *Journal of Basic Engineering* **87**, 977–985 (1965).
- ⁷⁸R. H. Mellen, “An Experimental Study of the Collapse of a Spherical Cavity in Water,” *The Journal of the Acoustical Society of America* **28**, 447–454 (1956).
- ⁷⁹V. A. Akulichev, Y. Y. Boguslavskii, A. I. Ioffe, and K. A. Naugol’nykh, “Radiation of finite-amplitude spherical waves,”

- Soviet Physics - Acoustics **13**, 281–285 (1968).
- ⁸⁰V. K. Kedrinskii, “Kirkwood-Bethe approximation for an underwater explosion with cylindrical symmetry,” *Combustion, Explosion, and Shock Waves* **8**, 94–100 (1972).
- ⁸¹K. J. Ebeling, “Zum Verhalten kugelförmiger, lasererzeugter Kavitationsblasen in Wasser,” *Acustica* **40**, 229–239 (1978).
- ⁸²K. Vokurka, “Comparison of Rayleigh’s, Herring’s, and Gilmore’s Models of Gas Bubbles,” *Acta Acustica united with Acustica* **59**, 214–219 (1986).
- ⁸³C. Herring, “Theory of the pulsations of the gas bubble produced by an underwater explosion,” Tech. Rep. Report No. 236 (Office of Scientific Research and Development, 1941).
- ⁸⁴L. Trilling, “The Collapse and Rebound of a Gas Bubble,” *Journal of Applied Physics* **23**, 14–17 (1952).
- ⁸⁵V. K. Kedrinskii and V. T. Kuzavov, “Dynamics of a Cylindrical Cavity in a Boundless Compressible Liquid,” in *Cavitation and Inhomogeneities in Underwater Acoustics*, edited by W. Lauterborn (Springer Berlin Heidelberg, Berlin, Heidelberg, 1980) pp. 119–124.
- ⁸⁶P. G. Tait, “Report on some of the physical properties of fresh water and sea water,” Tech. Rep. (1888).
- ⁸⁷L. D. Landau and E. M. Lifshitz, *Fluid Mechanics* (Pergamon Press Ltd., 1959).
- ⁸⁸O. Le Métayer and R. Saurel, “The Noble-Abel Stiffened-Gas equation of state,” *Physics of Fluids* **28**, 046102 (2016).
- ⁸⁹M. I. Radulescu, “Compressible flow in a Noble-Abel stiffened gas fluid,” *Physics of Fluids* **32**, 056101 (2020).
- ⁹⁰F. Denner, “The Gilmore-NASG model to predict single-bubble cavitation in compressible liquids,” *Ultrasonics Sonochemistry* **70**, 105307 (2021).
- ⁹¹M. H. Rice and J. M. Walsh, “Equation of State of Water to 250 Kilobars,” *The Journal of Chemical Physics* **26**, 824–830 (1957).
- ⁹²A. B. Arons, “Underwater Explosion Shock Wave Parameters at Large Distances from the Charge,” *The Journal of the Acoustical Society of America* **26**, 343–346 (1954).
- ⁹³J. R. McGrath, “Scaling Underwater Exploding Wires,” *Journal of Applied Physics* **37**, 4439–4443 (1966).
- ⁹⁴L. B. Poché, “Underwater Shock-Wave Pressures from Small Detonators,” *The Journal of the Acoustical Society of America* **51**, 1733–1737 (1972).
- ⁹⁵P. H. Rogers, “Weak-shock solution for underwater explosive shock waves,” *The Journal of the Acoustical Society of America* **62**, 1412–1419 (1977).
- ⁹⁶J. Best, *The Dynamics of Underwater Explosions*, Ph.D. thesis, University of Wollongong, Wollongong, Australia (1991).
- ⁹⁷F. Shan, Y. He, J.-J. Jiao, and H.-C. Wang, “Experimental and theoretical analysis of detonation products state on bubble dynamics and energy distribution in underwater explosion,” *Journal of Applied Physics* **130**, 174701 (2021).
- ⁹⁸J. Zhang, S. Wang, X. Jia, Y. Gao, and F. Ma, “An improved Kirkwood-Bethe model for calculating near-field shock-wave propagation of underwater explosions,” *AIP Advances* **11**, 035123 (2021).
- ⁹⁹L. Likhterov, “High-Frequency Acoustic Emission Generated by Underwater Explosion with Cylindrical Symmetry,” *Journal of Vibration and Acoustics* **122**, 140–142 (2000).
- ¹⁰⁰H.-Y. Kwak, K.-M. Kang, I. Ko, and J.-H. Kang, “Fire-ball expansion and subsequent shock wave propagation from explosives detonation,” *International Journal of Thermal Sciences* **59**, 9–16 (2012).
- ¹⁰¹S. Wang, Q. Gui, J. Zhang, Y. Gao, J. Xu, and X. Jia, “Theoretical and experimental study of bubble dynamics in underwater explosions,” *Physics of Fluids* **33**, 126113 (2021).
- ¹⁰²J. Zhang, S. Wang, X. Jia, Y. Gao, and F. Ma, “An engineering application of Prosperetti and Lezzi equation to solve underwater explosion bubbles,” *Physics of Fluids* **33**, 017118 (2021).
- ¹⁰³M.-K. Li, S.-P. Wang, S. Zhang, and H. Sagar, “Experimental study of underwater explosions below a free surface: Bubble dynamics and pressure wave emission,” *Physics of Fluids* **35**, 083313 (2023).
- ¹⁰⁴Z. Sheng, Y. Hao, J. Liu, H. Wang, Y. Gao, and F. Ma, “A shockwave calculation method for aluminized explosive of deep water explosion based on the Kirkwood-Bethe model,” *Propellants, Explosives, Pyrotechnics* **48**, e202200247 (2023).
- ¹⁰⁵D. Mavaleix-Marchessoux, *Modelling the Fluid-Structure Coupling Caused by a Far-Field Underwater Explosion*, Ph.D. thesis, Institut Polytechnique de Paris, Palaiseau, France (2020).
- ¹⁰⁶A. Ziolkowski, “A Method for Calculating the Output Pressure Waveform from an Air Gun,” *Geophysical Journal International* **21**, 137–161 (1970).
- ¹⁰⁷A. Ziolkowski, “Measurement of air-gun bubble oscillations,” *Geophysics* **63**, 2009–2024 (1998).
- ¹⁰⁸H. Bing-Shou, G. Hao, and H. Nan, “Simplified traditional bubble-motion equation and air-gun wavelet simulation based on a Van der Waals gas model,” *Applied Geophysics* **18**, 537–544 (2021).
- ¹⁰⁹M. Landrø and R. Sollie, “Source signature determination by inversion,” *Geophysics* **57**, 1633–1640 (1992).
- ¹¹⁰R. Laws, M. Landrø, and L. Amundsen, “An experimental comparison of three direct methods of marine source signature estimation,” *Geophysical Prospecting* **46**, 353–389 (1998).
- ¹¹¹H. O. Sertlek and G. Blacquiere, “Effects of the Rough Sea Surface on the Signature of a Single Air Gun,” *IEEE Journal of Oceanic Engineering* **44**, 575–581 (2019).
- ¹¹²D. Wehner, U. P. Svensson, and M. Landrø, “Acoustic signals in air and water generated by very shallow marine seismic sources: An experimental study,” *The Journal of the Acoustical Society of America* **147**, 1092–1103 (2020).
- ¹¹³I. Akhatov, O. Lindau, A. Topolnikov, R. Mettin, N. Vakhitova, and W. Lauterborn, “Collapse and rebound of a laser-induced cavitation bubble,” *Physics of Fluids* **13**, 2805–2819 (2001).
- ¹¹⁴A. Vogel, N. Linz, S. Freidank, and G. Paltauf, “Femtosecond-Laser-Induced Nanocavitation in Water: Implications for Optical Breakdown Threshold and Cell Surgery,” *Physical Review Letters* **100**, 038102 (2008).
- ¹¹⁵O. Supponen, D. Obreschkow, M. Tinguely, P. Kobel, N. Dor-saz, and M. Farhat, “Scaling laws for jets of single cavitation bubbles,” *Journal of Fluid Mechanics* **802**, 263–293 (2016).
- ¹¹⁶G. T. Bokman, L. Biasiori-Poulanges, B. Lukić, C. Bourquard, D. W. Meyer, A. Rack, and O. Supponen, “High-speed x-ray phase-contrast imaging of single cavitation bubbles near a solid boundary,” *Physics of Fluids* **35**, 013322 (2023).
- ¹¹⁷F. Reuter, T. Sato, V. Bellucci, S. Birnsteinova, C. Deiter, J. C. P. Koliyadu, R. Letrun, P. Villanueva-Perez, R. Bean, A. P. Mancuso, A. Meents, P. Vagovic, and C.-D. Ohl, “Laser-induced, single droplet fragmentation dynamics revealed through megahertz x-ray microscopy,” *Physics of Fluids* **35**, 113323 (2023).
- ¹¹⁸B. Zhao and O. Coutier-Delgosa, “The impacts of material acoustic impedance and thickness on single laser-induced bubble dynamics and determining factors in resulting pressure,” *Physics of Fluids* **35**, 103303 (2023).
- ¹¹⁹J. Mur, V. Agrež, J. Zevnik, R. Petkovšek, and M. Dular, “Microbubble collapse near a fiber: Broken symmetry conditions and a planar jet formation,” *Physics of Fluids* **35**, 023305 (2023).
- ¹²⁰X. Wang, G. Wu, J. Shen, Z. Sun, Y. Zhang, L. Zhang, and Y. Zhang, “Research on the collapse dynamics of a restricted cavitation bubble near a right-angle wall based on Kelvin impulse theory,” *Physics of Fluids* **35**, 073335 (2023).
- ¹²¹D. Mnich, F. Reuter, F. Denner, and C.-D. Ohl, “Single cavitation bubble dynamics in a stagnation flow,” *Journal of Fluid Mechanics* **979**, A18 (2024).
- ¹²²L. Fu, J. Wang, S. Wang, Z. Zhang, A. Vogel, X.-x. Liang, and C. Yao, “Secondary cavitation bubble dynamics during laser-induced bubble formation in a small container,” *Optics Express* **32**, 9747 (2024).
- ¹²³A. Vogel, S. Busch, and U. Parlitz, “Shock wave emission and cavitation bubble generation by picosecond and nanosecond optical breakdown in water,” *The Journal of the Acoustical Society of America* **100**, 148–165 (1996).

- ¹²⁴K.-T. Byun and H.-Y. Kwak, "A Model of Laser-Induced Cavitation," *Japanese Journal of Applied Physics* **43**, 621–630 (2004).
- ¹²⁵J. Oh, Y. Yoo, S. Seung, and H.-Y. Kwak, "Laser-induced bubble formation on a micro gold particle levitated in water under ultrasonic field," *Experimental Thermal and Fluid Science* **93**, 285–291 (2018).
- ¹²⁶S. Geng, Z. Yao, Q. Zhong, Y. Du, R. Xiao, and F. Wang, "Propagation of Shock Wave at the Cavitation Bubble Expansion Stage Induced by a Nanosecond Laser Pulse," *Journal of Fluids Engineering* **143**, 051209 (2021).
- ¹²⁷V. Agrež, J. Mur, J. Petelin, and R. Petkovšek, "Near threshold nucleation and growth of cavitation bubbles generated with a picosecond laser," *Ultrasonics Sonochemistry* **92**, 106243 (2023).
- ¹²⁸Z. Yang, H. Bao, L. Dai, H. Zhang, and J. Lu, "Experimental investigation of nanosecond laser-induced shock waves in water using multiple excitation beams," *Optics Express* **31**, 21845 (2023).
- ¹²⁹M. Vassholz, H. P. Hoeppe, J. Hagemann, J. M. Rosselló, M. Osterhoff, R. Mettin, T. Kurz, A. Schropp, F. Seiboth, C. G. Schroer, M. Scholz, J. Möller, J. Hallmann, U. Boesenberg, C. Kim, A. Zozulya, W. Lu, R. Shayduk, R. Schaffer, A. Madsen, and T. Salditt, "Pump-probe X-ray holographic imaging of laser-induced cavitation bubbles with femtosecond FEL pulses," *Nature Communications* **12**, 3468 (2021).
- ¹³⁰M. Vacher, G. Gimenez, and R. Goutte, "Nonlinear Behaviour of Microbubbles: Application to their Ultrasonic Detection," **54** (1984).
- ¹³¹M. Versluis, E. Stride, G. Lajoinie, B. Dollet, and T. Segers, "Ultrasound Contrast Agent Modeling: A Review," *Ultrasound in Medicine & Biology* **46**, 2117–2144 (2020).
- ¹³²F. Chavrier, J. Y. Chapelon, A. Gelet, and D. Cathignol, "Modeling of high-intensity focused ultrasound-induced lesions in the presence of cavitation bubbles," *The Journal of the Acoustical Society of America* **108**, 432–440 (2000).
- ¹³³S. K. Berlinda Law and Y. Zhou, "High-Intensity Focused Ultrasound Ablation by the Dual-Frequency Excitation," *IEEE Transactions on Ultrasonics, Ferroelectrics, and Frequency Control* **66**, 18–25 (2019).
- ¹³⁴M. Wang, Y. Lei, and Y. Zhou, "High-intensity focused ultrasound (HIFU) ablation by the frequency chirps: Enhanced thermal field and cavitation at the focus," *Ultrasonics* **91**, 134–149 (2019).
- ¹³⁵K. J. Pahk, D. K. Dhar, M. Malago, and N. Saffari, "Ultrasonic Histotripsy for Tissue Therapy," *Journal of Physics: Conference Series* **581**, 012001 (2015).
- ¹³⁶K. J. Pahk, P. Gélat, H. Kim, and N. Saffari, "Bubble dynamics in boiling histotripsy," *Ultrasound in Medicine & Biology* **44**, 2673–2696 (2018).
- ¹³⁷K. J. Pahk, M. O. De Andrade, P. Gélat, H. Kim, and N. Saffari, "Mechanical damage induced by the appearance of rectified bubble growth in a viscoelastic medium during boiling histotripsy exposure," *Ultrasonics Sonochemistry* **53**, 164–177 (2019).
- ¹³⁸D. L. Sokolov, *Dual Pulses for Cavitation Control in Lithotripsy: Shock Wave-Bubble Interactions and Bioeffects*, Ph.D. thesis, University of Washington, Seattle, WA, USA (2002).
- ¹³⁹E. Ayme and E. Carstensen, "Cavitation induced by asymmetric distorted pulses of ultrasound: Theoretical predictions," *IEEE Transactions on Ultrasonics, Ferroelectrics and Frequency Control* **36**, 32–40 (1989).
- ¹⁴⁰E. J. Aymé-Bellegarda, "Collapse and rebound of a gas-filled spherical bubble immersed in a diagnostic ultrasonic field," *The Journal of the Acoustical Society of America* **88**, 1054–1060 (1990).
- ¹⁴¹W. Kreider, L. A. Crum, M. R. Bailey, and O. A. Sapozhnikov, "A reduced-order, single-bubble cavitation model with applications to therapeutic ultrasound," *The Journal of the Acoustical Society of America* **130**, 3511–3530 (2011).
- ¹⁴²J. Gümmer, S. Schenke, and F. Denner, "Modelling Lipid-Coated Microbubbles in Focused Ultrasound Applications at Subresonance Frequencies," *Ultrasound in Medicine & Biology* **47**, 2958–2979 (2021).
- ¹⁴³Z. Li, Q. Zou, and D. Qin, "Enhancing cavitation dynamics and its mechanical effects with dual-frequency ultrasound," *Physics in Medicine & Biology* **67**, 085017 (2022).
- ¹⁴⁴D. Qin, S. Lei, X. Wang, X. Zhong, X. Ji, and Z. Li, "Resonance behaviors of encapsulated microbubbles oscillating nonlinearly with ultrasonic excitation," *Ultrasonics Sonochemistry* **94**, 106334 (2023).
- ¹⁴⁵J. H. Song, A. Moldovan, and P. Prentice, "Non-linear Acoustic Emissions from Therapeutically Driven Contrast Agent Microbubbles," *Ultrasound in Medicine & Biology* **45**, 2188–2204 (2019).
- ¹⁴⁶E. Zilonova, M. Solovchuk, and T. Sheu, "Bubble dynamics in viscoelastic soft tissue in high-intensity focal ultrasound thermal therapy," *Ultrasonics Sonochemistry* **40**, 900–911 (2018).
- ¹⁴⁷E. Zilonova, M. Solovchuk, and T. Sheu, "Simulation of cavitation enhanced temperature elevation in a soft tissue during high-intensity focused ultrasound thermal therapy," *Ultrasonics Sonochemistry* **53**, 11–24 (2019).
- ¹⁴⁸S. Bredihin, V. Andreev, A. Martekha, M. Schenzle, and I. Korotkiy, "Erosion potential of ultrasonic food processing," *Foods and Raw Materials* **9**, 335–344 (2021).
- ¹⁴⁹B. Glam, M. Strauss, S. Eliezer, and D. Moreno, "Shock compression and spall formation in aluminum containing helium bubbles at room temperature and near the melting temperature: Experiments and simulations," *International Journal of Impact Engineering* **65**, 1–12 (2014).
- ¹⁵⁰E. Sonde, T. Chaise, N. Boisson, and D. Nelias, "Modeling of cavitation peening: Jet, bubble growth and collapse, micro-jet and residual stresses," *Journal of Materials Processing Technology* **262**, 479–491 (2018).
- ¹⁵¹Z. Zhang, S. Wei, P. Wang, W. Qiu, and G. Zhang, "Progress in applications of laser induced cavitation on surface processing," *Optics & Laser Technology* **170**, 110212 (2024).
- ¹⁵²H. Huang, L. Qin, H. Tang, D. Shu, W. Yan, B. Sun, and J. Mi, "Ultrasound cavitation induced nucleation in metal solidification: An analytical model and validation by real-time experiments," *Ultrasonics Sonochemistry* **80**, 105832 (2021).
- ¹⁵³H. Huang, H. Tu, H. Xu, P. Shi, and D. Wang, "Insight of external ultrasound on energy-production acceleration from renewable Al-water reaction in Al-based metallic materials," *International Journal of Hydrogen Energy* **48**, 20253–20263 (2023).
- ¹⁵⁴M. Rakita and Q. Han, "Influence of Pressure Field in Melts on the Primary Nucleation in Solidification Processing," *Metallurgical and Materials Transactions B* **48**, 2232–2244 (2017).
- ¹⁵⁵V. Minsier and J. Proost, "Shock wave emission upon spherical bubble collapse during cavitation-induced megasonic surface cleaning," *Ultrasonics Sonochemistry* **15**, 598–604 (2008).
- ¹⁵⁶V. K. Kedrinskii, "Creation of special shock tubes and investigation of cumulation of liquid cylindrical shells in a rotating system," *Journal of Applied Mechanics and Technical Physics* **63**, 1–6 (2022).
- ¹⁵⁷M. P. Brenner, S. Hilgenfeldt, and D. Lohse, "Single-bubble sonoluminescence," *Reviews of Modern Physics* **74**, 425–484 (2002).
- ¹⁵⁸G. Gimenez, "The simultaneous study of light emissions and shock waves produced by cavitation bubbles," *The Journal of the Acoustical Society of America* **71**, 839–846 (1982).
- ¹⁵⁹H. Nazari-Mahroo, K. Pasandideh, H. A. Navid, and R. Sadighi-Bonabi, "Influence of liquid compressibility on the dynamics of single bubble sonoluminescence," *Physics Letters A* **382**, 1962–1967 (2018).
- ¹⁶⁰H. P. Hoeppe, M. Osterhoff, A. Aghel Maleki, J. M. Rosselló, M. Vassholz, J. Hagemann, T. Engler, D. Schwarz, A. Rodriguez-Fernandez, U. Boesenberg, J. Möller, R. Shayduk, J. Hallmann, A. Madsen, R. Mettin, and T. Salditt, "The collapse of a sonoluminescent cavitation bubble imaged with X-ray free-electron laser pulses," *New Journal of Physics* **26**, 033002 (2024).

- ¹⁶¹Y.-P. Lee, S. W. Karng, J.-S. Jeon, and H.-Y. Kwak, "Shock Pulse from a Sonoluminescing Gas Bubble," *Journal of the Physical Society of Japan* **66**, 2537–2540 (1997).
- ¹⁶²J. Holzfuss, M. Rüggeberg, and A. Billo, "Shock Wave Emissions of a Sonoluminescing Bubble," *Physical Review Letters* **81**, 5434–5437 (1998).
- ¹⁶³J. Holzfuss, "Acoustic energy radiated by nonlinear spherical oscillations of strongly driven bubbles," *Proceedings of the Royal Society A: Mathematical, Physical and Engineering Sciences* **466**, 1829–1847 (2010).
- ¹⁶⁴A. Shima, "The Natural Frequency of a Bubble Oscillating in a Viscous Compressible Liquid," *Journal of Basic Engineering* **92**, 555–561 (1970).
- ¹⁶⁵C. Hunter, "On the collapse of an empty cavity in water," *Journal of Fluid Mechanics* **8**, 241–263 (1960).
- ¹⁶⁶V. A. Akulichev, "Pulsation of cavitation voids," in *High-Intensity Ultrasonic Fields*, edited by L. D. Rozenberg (Springer US, Boston, MA, 1971).
- ¹⁶⁷V. S. Moholkar, S. Rekveld, and M. M. Warmoeskerken, "Modeling of the acoustic pressure fields and the distribution of the cavitation phenomena in a dual frequency sonic processor," *Ultrasonics* **38**, 666–670 (2000).
- ¹⁶⁸D. Fuster, C. Dopazo, and G. Hauke, "Liquid compressibility effects during the collapse of a single cavitating bubble," *The Journal of the Acoustical Society of America* **129**, 122–131 (2011).
- ¹⁶⁹M. Mahdi, M. Shams, and R. Ebrahimi, "Effects of heat transfer on the strength of shock waves emitted upon spherical bubble collapse," *International Journal of Numerical Methods for Heat & Fluid Flow* **20**, 372–391 (2010).
- ¹⁷⁰D. B. Preso, D. Fuster, A. B. Sieber, D. Obreschkow, and M. Farhat, "Vapor compression and energy dissipation in a collapsing laser-induced bubble," *Physics of Fluids* **36**, 033342 (2024).
- ¹⁷¹X. Zhang, C. Yang, C. Wang, Y. Zhang, and Y. Zhang, "Dynamics of an oscillating cavitation bubble within a narrow gap," *Physics of Fluids* **35**, 103302 (2023).
- ¹⁷²L. Likhterov, "High-frequency acoustic noise emitted by initial impact of solid sphere falling onto liquid surface," *Physics of Fluids* **10**, 321–323 (1998).
- ¹⁷³A. Berman and L. Likhterov, "Spectrum asymptotics of high-frequency acoustic emission generated by surface explosion," *Physics of Fluids* **13**, 1508–1512 (2001).
- ¹⁷⁴Y. C. Kim, P. Blanloeuil, D. D. Li, R. A. Taylor, and T. J. Barber, "Acoustically driven translation of a single bubble in pulsed traveling ultrasonic waves," *Physics of Fluids* **35**, 033315 (2023).
- ¹⁷⁵J. B. Keller and I. I. Kolodner, "Damping of Underwater Explosion Bubble Oscillations," *Journal of Applied Physics* **27**, 1152–1161 (1956).
- ¹⁷⁶A. Prosperetti, "Bubble phenomena in sound fields: Part one," *Ultrasonics* **22**, 69–77 (1984).
- ¹⁷⁷L. Rayleigh, "Aerial plane waves of finite amplitude," *Proceedings of the Royal Society of London. Series A* **84**, 247–284 (1910).
- ¹⁷⁸R. J. LeVeque, *Numerical Methods for Conservation Laws*, 2nd ed., Lectures in Mathematics (Birkhäuser, Basel Berlin, 2008).
- ¹⁷⁹D. L. Chapman, "VI. On the rate of explosion in gases," *The London, Edinburgh, and Dublin Philosophical Magazine and Journal of Science* **47**, 90–104 (1899).
- ¹⁸⁰E. Jouguet, "Sur la propagation des réactions chimiques dans les gaz," *Journal de Mathématiques Pures et Appliquées* **1**, 347–425 (1905).
- ¹⁸¹B. Riemann, "Über die Fortpflanzung ebener Luftwellen von endlicher Schwingungsweite," *Abhandlungen der Königlichen Gesellschaft der Wissenschaften zu Göttingen* **8** (1860).
- ¹⁸²L. E. Kinsler, ed., *Fundamentals of Acoustics*, 4th ed. (Wiley, New York, 2000).
- ¹⁸³R. H. Randall, *An Introduction to Acoustics*, dover ed. (Dover Publications, Mineola, N.Y., 2005).
- ¹⁸⁴V. K. Kedrinskii, *Hydrodynamics of Explosions: Experiment and Models* (Springer, Berlin, Heidelberg, New York, 2005).
- ¹⁸⁵D. T. Blackstock, "On Plane, Spherical, and Cylindrical Sound Waves of Finite Amplitude in Lossless Fluids," *The Journal of the Acoustical Society of America* **36**, 217–219 (1964).
- ¹⁸⁶A.-M. Zhang, S.-M. Li, P. Cui, S. Li, and Y.-L. Liu, "A unified theory for bubble dynamics," *Physics of Fluids* **35**, 033323 (2023).
- ¹⁸⁷W. Wagner and A. Pruß, "The IAPWS Formulation 1995 for the Thermodynamic Properties of Ordinary Water Substance for General and Scientific Use," *Journal of Physical and Chemical Reference Data* **31**, 387–535 (2002).
- ¹⁸⁸F. Harlow and A. Amsden, "Fluid dynamics," Monograph LA-4700 (Los Alamos National Laboratory, 1971).
- ¹⁸⁹O. Le Métayer, J. Massoni, and R. Saurel, "Élaboration des lois d'état d'un liquide et de sa vapeur pour les modèles d'écoulements diphasiques," *International Journal of Thermal Sciences* **43**, 265–276 (2004).
- ¹⁹⁰J. Chandran and A. Salih, "A modified equation of state for water for a wide range of pressure and the concept of water shock tube," *Fluid Phase Equilibria* **483**, 182–188 (2019).
- ¹⁹¹G. Tammann, "Über Zustandsgleichungen im Gebiete kleiner Volumen," *Annalen der Physik* **342**, 975–1013 (1912).
- ¹⁹²G. M. Kontogeorgis, R. Privat, and J.-N. Jaubert, "Taking Another Look at the van der Waals Equation of State—Almost 150 Years Later," *Journal of Chemical & Engineering Data* **64**, 4619–4637 (2019).
- ¹⁹³E. A. Neppiras, "Acoustic cavitation," *Physics Reports* **61**, 159–251 (1980).
- ¹⁹⁴P. M. Tilmann, "Nonlinear Sound-Scattering by Small Bubbles," in *Cavitation and Inhomogeneities in Underwater Acoustics*, edited by W. Lauterborn (Springer Berlin Heidelberg, Berlin, Heidelberg, 1980) pp. 113–118.
- ¹⁹⁵Y. A. Ilinskii, E. A. Zabolotskaya, T. A. Hay, and M. F. Hamilton, "Models of cylindrical bubble pulsation," *The Journal of the Acoustical Society of America* **132**, 1346–1357 (2012).
- ¹⁹⁶F. Denner and S. Schenke, "APECSS: A software library for cavitation bubble dynamics and acoustic emissions," *Journal of Open Source Software* **8**, 5435 (2023).
- ¹⁹⁷I. Johnston, "The Noble-Abel Equation of State: Thermodynamic Derivations for Ballistics Modelling," Tech. Rep. Technical Report DSTO-TN-0670 (Defence Science and Technology Organisation, 2005).
- ¹⁹⁸E. F. Toro, *Riemann Solvers and Numerical Fluid Dynamics: A Practical Introduction*, 3rd ed. (Springer, 2009).
- ¹⁹⁹A. Prosperetti, L. A. Crum, and K. W. Commander, "Nonlinear bubble dynamics," *The Journal of the Acoustical Society of America* **83**, 502–514 (1988).
- ²⁰⁰D. Qin, S. Lei, B. Chen, Z. Li, W. Wang, and X. Ji, "Numerical investigation on acoustic cavitation characteristics of an air-vapor bubble: Effect of equation of state for interior gases," *Ultrasonics Sonochemistry* **97**, 106456 (2023).
- ²⁰¹H. Nazari-Mahroo, K. Pasandideh, H. Navid, and R. Sadighi-Bonabi, "Influence of liquid density variation on the bubble and gas dynamics of a single acoustic cavitation bubble," *Ultrasonics* **102**, 106034 (2020).
- ²⁰²A. Prosperetti, "The thermal behaviour of oscillating gas bubbles," *Journal of Fluid Mechanics* **222**, 587 (1991).
- ²⁰³L. Stricker, A. Prosperetti, and D. Lohse, "Validation of an approximate model for the thermal behavior in acoustically driven bubbles," *The Journal of the Acoustical Society of America* **130**, 3243–3251 (2011).
- ²⁰⁴G. Zhou and A. Prosperetti, "Modelling the thermal behaviour of gas bubbles," *Journal of Fluid Mechanics* **901**, R3 (2020).
- ²⁰⁵G. Zhou, "Modeling the thermal behavior of an acoustically driven gas bubble," *The Journal of the Acoustical Society of America* **149**, 923–933 (2021).
- ²⁰⁶E. Samiei, M. Shams, and R. Ebrahimi, "Numerical Study on Mass Transfer Effects on Spherical Cavitation Bubble Collapse in an Acoustic Field," in *ASME 2010 10th Biennial Confer-*

- ence on Engineering Systems Design and Analysis, Volume 3 (ASMEDC, Istanbul, Turkey, 2010) pp. 425–433.
- ²⁰⁷E. L. Lee, H. C. Hornig, and J. W. Kury, “Adiabatic Expansion Of High Explosive Detonation Products,” Tech. Rep. UCRL-50422 (Univ. of California Radiation Lab. at Livermore, Livermore, CA, USA, 1968).
- ²⁰⁸G. Baudin and R. Serradeill, “Review of Jones-Wilkins-Lee equation of state,” *EPJ Web of Conferences* **10**, 00021 (2010).
- ²⁰⁹M. Riley, “Analytical Solutions for Predicting Underwater Explosion Gas Bubble Behaviour,” Tech. Rep. DRDC Atlantic TM 2010-237 (Defence R&D Canada – Atlantic, Dartmouth, NS, Canada, 2010).
- ²¹⁰Y. Gao, S. Wang, J. Zhang, X. Jia, C. Liang, and F. Ma, “Effects of underwater explosion depth on shock wave overpressure and energy,” *Physics of Fluids* **34**, 037108 (2022).
- ²¹¹X. Jia, S. Wang, J. Xu, J. Zhang, Y. Gao, and F. Ma, “Non-linear characteristics and corrections of near-field underwater explosion shock waves,” *Physics of Fluids* **34**, 046108 (2022).
- ²¹²A. Prosperetti and A. Lezzi, “Bubble dynamics in a compressible liquid. Part 1. First-order theory,” *Journal of Fluid Mechanics* **168**, 457–478 (1986).
- ²¹³A. Lezzi and A. Prosperetti, “Bubble dynamics in a compressible liquid. Part 2. Second-order theory,” *Journal of Fluid Mechanics* **185**, 289–321 (1987).
- ²¹⁴T. B. Benjamin, “Pressure waves from collapsing cavities,” in *Second Symposium on Naval Hydrodynamics: Hydrodynamic Noise, Cavity Flow*, edited by R. Cooper (National Academy of Sciences–National Research Council, 1958).
- ²¹⁵J. B. Keller and M. Miksis, “Bubble oscillations of large amplitude,” *The Journal of the Acoustical Society of America* **68**, 628–633 (1980).
- ²¹⁶X. Wang, X. Zhang, S. Li, C. Zhang, Y. Zhang, Q. Jiang, J. Li, S. Zheng, and Y. Zhang, “Primary resonance characteristics of a cylindrical bubble based on the multi-scale method,” *Physics of Fluids* **36**, 023333 (2024).
- ²¹⁷J. Dormand and P. Prince, “A family of embedded Runge-Kutta formulae,” *Journal of Computational and Applied Mathematics* **6**, 19–26 (1980).
- ²¹⁸R. D. Fay, “Plane sound waves of finite amplitude,” *The Journal of the Acoustical Society of America* **3**, 222–241 (1931).
- ²¹⁹M. F. Hamilton and D. T. Blackstock, “On the coefficient of non-linearity β in nonlinear acoustics,” *The Journal of the Acoustical Society of America* **83**, 74–77 (1988).
- ²²⁰K. A. Naugol’nykh, “Absorption of finite-amplitude waves,” in *High-Intensity Ultrasonic Fields*, edited by L. D. Rozenberg (Springer US, Boston, MA, 1971).
- ²²¹I. Rudnick, “Theory of the Attenuation of Very High Amplitude Sound Waves,” Tech. Rep. (Soundrive Engine Company, Los Angeles, California, USA, 1952).
- ²²²C. B. Laney, *Computational Gasdynamics* (Cambridge University Press, Cambridge; New York, NY, 1998).
- ²²³S. Schenke, F. Sewerin, B. van Wachem, and F. Denner, “Explicit predictor–corrector method for nonlinear acoustic waves excited by a moving wave emitting boundary,” *Journal of Sound and Vibration* **527**, 116814 (2022).
- ²²⁴G. B. Whitham, *Linear and Nonlinear Waves* (John Wiley & Sons, Inc., Hoboken, NJ, USA, 1999).
- ²²⁵D. T. Blackstock, “Connection between the Fay and Fubini Solutions for Plane Sound Waves of Finite Amplitude,” *The Journal of the Acoustical Society of America* **39**, 1019–1026 (1966).
- ²²⁶W. Lauterborn, T. Kurz, and I. Akhatov, “Nonlinear Acoustics in Fluids,” in *Springer Handbook of Acoustics*, edited by T. D. Rossing (Springer New York, New York, NY, 2007) pp. 257–297.
- ²²⁷L. Rayleigh, “On the pressure developed in a liquid during the collapse of a spherical cavity,” *Philosophical Magazine* **34**, 94–98 (1917).
- ²²⁸G. ter Haar, “Ultrasonic imaging: Safety considerations,” *Interface Focus* **1**, 686–697 (2011).
- ²²⁹Y. Fan, H. Li, and D. Fuster, “Time-delayed interactions on acoustically driven bubbly screens,” *The Journal of the Acoustical Society of America* **150**, 4219–4231 (2021).
- ²³⁰L. Fu, X.-X. Liang, S. Wang, S. Wang, P. Wang, Z. Zhang, J. Wang, A. Vogel, and C. Yao, “Laser induced spherical bubble dynamics in partially confined geometry with acoustic feedback from container walls,” *Ultrasonics Sonochemistry* , 106664 (2023).